MECHATRONIC DESIGN OF A MODULAR THREE-AXIS SLIDER SYSTEM FOR HIGH-PRECISION POSITIONING APPLICATIONS

A THESIS

SUBMITTED TO THE DEPARTMENT OF MECHANICAL

ENGINEERING

AND THE GRADUATE SCHOOL OF ENGINEERING AND SCIENCE

OF BILKENT UNIVERSITY

IN PARTIAL FULFILLMENT OF THE REQUIREMENTS

FOR THE DEGREE OF

MASTER OF SCIENCE

By

Erva Ulu

August, 2012

I certify that I have read this thesis and that in my opinion it is fully adequate, in scope and in quality, as a thesis for the degree of Master of Science.

Assist. Prof. Dr. Melih Çakmakçı (Advisor)

I certify that I have read this thesis and that in my opinion it is fully adequate, in scope and in quality, as a thesis for the degree of Master of Science.

Assist. Prof. Dr. Yiğit Karpat

I certify that I have read this thesis and that in my opinion it is fully adequate, in scope and in quality, as a thesis for the degree of Master of Science.

Prof. Dr. Hitay Özbay

Approved for the Graduate School of Engineering and Science:

Prof. Dr. Levent Onural
Director of the Graduate School

ABSTRACT

MECHATRONIC DESIGN OF A MODULAR THREE-AXIS SLIDER SYSTEM FOR HIGH-PRECISION POSITIONING APPLICATIONS

Erva Ulu
M.S. in Mechanical Engineering
Supervisor: Assist. Prof. Dr. Melih Çakmakçı
August, 2012

Following the recent improvements in precision engineering related technology, interest for micro/nano-engineering applications are increased and various micro/nano-scale operations and products are developed. For micro/nano-scale applications, high-precision equipment including micro/nano-positioning devices with high accuracy and precision are required. In this thesis, mechatronic design of a three axes micro/nano-positioning device is discussed in detail. In order to satisfy nanometer level precision, an adaptive method to increase the available measurement resolution of quadrature encoders is presented.

Performance characteristics of micro/nano-positioning devices usually include positioning accuracy of their each individual axis, operation range, maximum velocity and maximum acceleration. For this reason, permanent magnet linear motors (PMLM) are chosen as actuators in the presented design due to their outstanding characteristics. Moreover, in order to provide high-flexibility in terms of applications and simplify the control of the system, modularity is one of the main concerns while designing the micro/nano-positioning system presented here. Building the modular single axis slider system, three axes positioning device is constructed by assembling three of them perpendicularly. In this design, linear optical encoders are used as feedback sensors. Movement range of the designed system is $120mm$ in each direction.

Since the available linear optical encoders have measurement resolution of $1\mu m$, resolution of them is to be improved in software for sub-micron level positioning applications. For this purpose, a new method to increase the available measurement resolution of quadrature encoders is presented in this thesis. This method features an adaptive signal correction phase and an interpolation phase.

Imperfections in the encoder signals including amplitude differences, mean offsets and quadrature phase shift errors are corrected by using recursive least squares (RLS) with exponential forgetting and resetting. Interpolation of the corrected signals is accomplished by a quick access look-up table calculated offline to satisfy linear mapping from available sinusoidal signals to higher order ones. With the conversion of the high-order sinusoids to binary pulses, position information is derived. By using the presented method, $10nm$ measurement resolution is achieved with an encoder with $1\mu m$ off-the-shelf resolution. Experiment results demonstrating the effectiveness of the proposed method are presented. Validation of the method is accomplished for several cases including the best resolution obtained. Practical constraints limiting the maximum interpolation number are also discussed in detail.

Keywords: Precision positioning, encoder resolution, adaptive systems, measurement interpolation, quadrature encoder signals, modular design.

ÖZET

YÜKSEK HASSASİYETLİ POZİSYONLAMA UYGULAMALARI İÇİN MODÜLER ÜÇ-EKSENLİ KIZAK SİSTEMİNİN MEKATRONİK TASARIMI

Erva Ulu
Makine Mühendisliği, Yüksek Lisans
Tez Yöneticisi: Assist. Prof. Dr. Melih Çakmakçı
Ağustos, 2012

Hassas mühendislik alanındaki teknolojik ilerlemeyi takiben mikro/nano-mühendislik uygulamalarına olan ilgi artmış, son yıllarda mikro/nano-boyutlu birçok süreç ve ürün geliştirilmiştir. Mikro/nano boyutlarda işlem yapabilmek için kullanılacak makinaların yüksek doğruluk ve hassasiyete sahip mikro/nano-pozisyonlama cihazları içermesi gerekmektedir. Bu tezde bir üç eksenli mikro/nano-pozisyonlama cihazının mekatronik tasarımı detaylı bir biçimde anlatılmaktadır. Ayrıca, nanometre seviyesinde hassasiyet değerlerine ulaşabilmek için dört evreli enkoderlerin mevcut çözünürlük değerlerinin arttırılmasını sağlayan uyarlamalı bir metod sunulmaktadır.

Mikro/nano-pozisyonlama cihazlarının performans karakteristiği genellikle eksenlerin konumlama hassasiyetleri, hareket aralığı, maksimum hız ve ivmelenmeleri olmaktadır. Bu sebeple, bu tezde bahsedilen tasarımda eyleyici olarak üstün karakteristiklerinden dolayı sürekli mıknatıs lineer motorlar (PMLM) seçilmiştir. Ayrıca, kullanıcıya uygulamalarda esneklik sağlaması ve sistem kontrolünü kolaylaştırması amacıyla burada sunulan mikro/nano-pozisyonlama sisteminin tasarımı yapılırken modülerite ana kriterler arasında tutulmuştur. Modüler tek eksenli kızak sisteminin tasarımından sonra bu kızaklardan üç tanesinin birbirine dik olarak montajı ile üç eksenli pozisyonlama cihazı oluşturulmuştur. Bu tasarımda geri besleme sensörü olarak lineer optik enkoderler kullanılmıştır. Geliştirilen sistemin hareket aralığı her eksende $120mm$'dir.

Mevcut lineer optik enkoderlerin ölçüm çözünürlükleri $1\mu m$ olduğundan mikron altı seviyelerdeki pozisyonlama uygulamaları için enkoderlerin çözünürlükleri yazılım üzerinde arttırılmalıdır. Bu amaçla, dört evreli enkoderlerin mevcut

çözünürlüklerini arttırmak üzere geliştirilen yeni bir metod bu tezde sunulmaktadır. Bu metod uyarlamalı sinyal düzeltme ve interpolasyon aşamalarından oluşmaktadır. Enkoder sinyallerindeki büyüklük farkları, ortalama değer sapmaları ve dört evreli faz farkı hataları üssel unutmalı ve sıfırlamalı tekrarlamalı en küçük kareler yöntemi (RLS) kullanılarak düzeltilmektedir. Düzeltilmiş sinyallerin interpolasyonu ise çevrim dışı oluşturulmuş bir hızlı erişimli taramalı tablo sayesinde yapılmaktadır. Bu tablo ile orijinal enkoder sinyalleri ile yüksek dereceli sinüzoidler arasında doğrusal eşleştirme yapılmıştır. Yüksek dereceli sinüzoidlerin ikili pulslara dönüştürülmesi sonucunda pozisyon bilgisi elde edilmiş olur. Sunulan metod kullanılarak $1\mu m$ orijinal çözünürlüğü olan bir enkoder ile $10nm$'lik ölçüm çözünürlüğü elde edilmiştir. Önerilen metodun etkinliğini gösteren deneyler tez içerisinde verilmiştir. Metodun doğrulaması elde edilen en yüksek çözünürlük dahil olmak üzere çeşitli çözünürlük değerleri için başarıyla yapılmıştır. Maksimum interpolasyon sayısını sınırlandıran pratikteki kısıtlamalar da detaylıca incelenmiştir.

Anahtar sözcükler: Hassas pozisyonlama, enkoder hassasiyeti, uyarlamalı sistemler, ölçüm aradeğerlemesi, dört evreli enkoder sinyalleri, modüler dizayn.

Acknowledgement

I would like to thank my advisor, Assist. Prof. Melih Çakmakcı. His guidance, support and encouragement have been crucial to my successful completion of all the work contained in this thesis.

I would also like to thank Assist. Prof. Sinan Filiz for his valuable advice and help throughout this study.

I wish to give my thanks to members of Bilkent University Mechanical Engineering Department and the thesis committee.

I would also acknowledge the help of the undergraduate students working in our lab, Ersun Sozen and Oytun Ugurel.

I would also like to thank The Scientific and Technology Research Council of Turkey (TÜBİTAK) for the support of this research through grants and I am also grateful to TÜBİTAK for National Scholarship for Master of Science Students (TÜBİTAK - 2210 Yurt İçi Yüksek Lisans Bursu).

I am also thankful to my family and friends for their love, support and encouragement.

Lastly, but most importantly I would like to express my special thanks to my wife, Nurcan Geçer Ulu.

Contents

1 Introduction **1**

2 Background Information **5**

2.1 Micro/Nano-Positioning Systems 5

2.2 Encoder Resolution Improvement Methods 8

3 Design of Micro/Nano-Positioning Device **12**

3.1 Modular Single-Axis Slider System 12

3.1.1 Components and Control Setup 14

3.1.2 Design Improvements of Mechanical Components 18

3.2 Assembly Configurations of Modular Slider 24

3.3 Three-Axis Slider System 26

3.3.1 Counter Balance Subsystem 26

3.3.2 Manufacturing and Assembly Tolerances 28

4 Encoder Resolution Improvement Method **31**

4.1 Overview of the Proposed Approach 32

4.2 Adaptive Encoder Signal Correction (Step 1) 35

4.3 Look-up Table Based Signal Interpolation (Step 2) 40

4.4 Binary Pulse Generation and Position Information 46

4.5 Practical Limitations 48

5 Real-Time Implementation 50

5.1 Real-Time Implementation of Encoder Resolution Improvement Method 51

5.2 Real-Time Implementation of Overall Control System 55

6 Validation and Experiments 58

6.1 Validation of Encoder Resolution Improvement Method 59

6.1.1 Experimental Setup 59

6.1.2 Validation Test Results 61

6.2 Experimental Results 65

7 Conclusion and Future Works 73

A Labview Implementations 80

List of Figures

1.1 Closed Loop System Setup of a Typical Positioning Device 2

2.1 Ballscrew Mechanism [1] 6

2.2 Piezoelectric Actuator [2] 7

2.3 Permanent Magnet Linear Motor [3] 8

2.4 Ideal and Interpolated Encoder Signals 9

2.5 Exaggerated Illustration of Original Encoder Signals 10

3.1 3D Drawing of Three-Axis Positioning System 13

3.2 3D Drawing of Single-Axis Slider 13

3.3 Top View of the Designed Single Axis Slider 14

3.4 Bottom View of the Designed Single Axis Slider 15

3.5 Single Axis Slider with its Components 17

3.6 Closed Loop Control System Setup of the Single Axis Slider . . . 17

3.7 Photograph of Testbed for the Single Axis Slider 18

3.8 (a) Top and (b) Bottom View of the Previous Single Axis Slider Design 19

3.9 Moving Sliders and Stationary Bottom Bases of (a) Previous and (b) New Single Axis Slider Designs 20

3.10 (a) Previous and (b) New Scale Holder Designs 21

3.11 Safety Pins on Encoder Scale Holder 22

3.12 Single Axis Slider 22

3.13 Example Single Axis Assembly Configurations with a One, (b) Two and (c) Three Sliders 23

3.14 Example Two Axis Assembly Configurations Using Two Sliders in a X-Y (b) Oblique X-Y and (c) X-Z Arrangements 23

3.15 Example Two Axis Assembly Configurations Using Three Sliders in a X-Y (b) Oblique X-Y and (c) X-Z Arrangements 24

3.16 Example Three Axis Assembly Configurations Using Three Sliders in a X-Y-Z (b) Oblique X-Y-Z Arrangements 25

3.17 Two Axis Slider System 26

3.18 Three Axis Micro/Nano-Positioning System 27

3.19 Counter Balance Subsystem 28

3.20 (a) Tolerance Critical Sections of Single Axis Slider with Detail Views of (b) Section A and (c) Section B 29

4.1 General Flow Diagram of the Proposed Approach 33

4.2 Encoder Signal Parameters Recorded Through 120mm Motion of the Single Axis Slider 38

4.3 Corrected Encoder Signals Using RLS (a) with and (b) without Resetting 39

4.4 Corrected and Original Encoder Signals 40

4.5 Verification of Quadrature Phase Difference Between Corrected Signals 41

4.6 Interpolation Results for $n = 25$ 45

4.7 Variation of Index Number for $n = 25$ 45

4.8 Binary Pulses Obtained for $n = 25$ 47

4.9 Example Showing Encoder Signals and Binary Pulses for (a) Without Interpolation (b) With Interpolation Cases 48

5.1 Encoder Resolution Improvement Method Labview Implementation 51

5.2 Encoder Signal Correction Labview Implementation 52

5.3 Look-up Table Based Interpolation Labview Implementation . . . 54

5.4 Binary Pulse Generation and Position Information Derivation Labview Implementation 55

5.5 Labview Implementation of Overall Control System for Single Axis Slider System 56

5.6 Labview Implementation of Control Loop for Single Axis Slider System 56

6.1 Testbed for Validation Experiments 60

6.2 Validation Results on x-Axis Slider for Interpolation Number of $n = 10$ Resulting $100nm$ Measurement Resolution 62

6.3 Validation Results on x-Axis Slider for Interpolation Number of $n = 50$ Resulting $20nm$ Measurement Resolution 62

6.4 Validation Results on x-Axis Slider for Interpolation Number of $n = 100$ Resulting $10nm$ Measurement Resolution 62

6.5 Validation Results on y-Axis Slider for Interpolation Number of $n = 10$ Resulting $100nm$ Measurement Resolution 63

6.6 Validation Results on y-Axis Slider for Interpolation Number of $n = 50$ Resulting $20nm$ Measurement Resolution 63

6.7 Validation Results on y-Axis Slider for Interpolation Number of $n = 100$ Resulting $10nm$ Measurement Resolution 63

6.8 Validation Results on z-Axis Slider for Interpolation Number of $n = 10$ Resulting $100nm$ Measurement Resolution 64

6.9 Validation Results on z-Axis Slider for Interpolation Number of $n = 50$ Resulting $20nm$ Measurement Resolution 64

6.10 Validation Results on z-Axis Slider for Interpolation Number of $n = 100$ Resulting $10nm$ Measurement Resolution 64

6.11 Interpolation Results for $n = 16$ 66

6.12 Interpolation Results for $n = 50$ 66

6.13 Interpolation Results for $n = 100$ 67

6.14 Tracking Performance of the Single Axis Slider 67

6.15 Reference Input Trajectory for Two-Axis Slider System 68

6.16 Tracking, (a) and (b), and Contouring, (c), Performance of Two-Axis Positioning System 69

6.17 Three Dimensional Reference Input Trajectory for Three-Axis Slider System 70

6.18 Tracking, (a), (b)and (c), and Contouring, (c), Performance of Three-Axis Positioning System 72

A.1 Labview Front Panel for Single Axis Slider 80

A.2 Labview Front Panel for Two-Axis Slider System 81

A.3 Labview Implementation of Overall Control System for Two-Axis Slider System 82

A.4 Labview Front Panel for Three-Axis Slider System 83

A.5 Labview Implementation of Overall Control System for Three-Axis Slider System 84

List of Tables

3.1 Specifications of BLMUC-95 Linear Motor 16

4.1 A Generic Look-up Table 42

4.2 Index Calculation Table 44

Chapter 1

Introduction

There is a growing interest for precision positioning systems from various micro/nano-technology applications [4]. Micro/nano manufacturing and assembly, optical component alignment systems, scanning microscopy applications, nano-particle placement applications, biotechnology applications and cell/tissue engineering are some examples of the applications that precision positioning devices are commonly used [5, 6, 7]. High precision positioning devices are required for any operations in micro/nano-scale applications. Performance characteristics of these devices depend on positioning accuracy, maximum velocity and acceleration that they can operate with acceptable performance based on the application. These characteristics are mostly determined by the actuator that gives motion to the slider and the feedback sensor that supplies the position information.

Commonly used actuators for micro/nano-positioning systems are piezoelectric actuators [8, 9, 10], ballscrew mechanisms [5, 11] and permanent magnet linear motors (PMLM) [11, 12]. Piezoelectric actuators have the motion range of just tens of micrometers and they are limited in terms of acceleration and velocity capabilities [5]. Also, for a ballscrew mechanism, a ballscrew is coupled with a DC motor to convert the motor rotary motion into linear motion. Thus, ballscrew driven mechanisms have accuracy limitations due to backlash and wear of the mechanical components, and their acceleration and velocity capabilities are limited as a result of the ballscrew mechanism [12]. On the other hand, linear

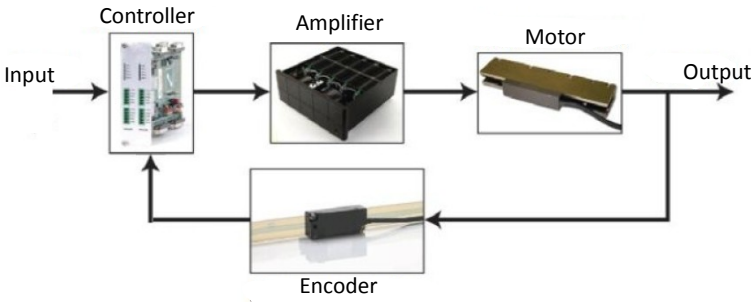

Figure 1.1: Closed Loop System Setup of a Typical Positioning Device

motors are gaining popularity for precision positioning applications due to their superior characteristics. Due to their designs, there is no contact between the stationary and moving parts of PMLMs. Hence, backlash or wear is not concern and nonlinearity due to the contact mechanism is also eliminated. With the linear motors, high acceleration and velocity values can be achieved in long ranges (greater than $100mm$).

As feedback sensors, high-resolution sensors are required in micro/nano-positioning systems in order to satisfy high-precision. Commonly used sensors are laser interferometers, capacitive sensors and optical encoders [12, 13]. Although laser interferometers and capacitive sensors can reach up to sub-nanometer level measurement resolutions, their sensing range is limited to micrometer level [14, 13]. Conversely, measurement ranges of linear optical encoders are higher (hundreds of milimeters) but their resolutions are usually in micrometer level [15].

In this thesis, the main objective is to design a three-axis micro/nano-positioning device that can operate in long ranges ($120mm\ x\ 120mm\ x\ 120mm$). Due to their outstanding characteristics PMLM is used as the actuator in single axis slider design. Moreover, linear optical encoders are used as feedback sensors since their measurement range is suitable for the desired system. For the design process, modularity is one of the main concerns in order to provide high flexibility in terms of applications and simplify the control of the system. For this purpose, the three-axis positioning system is designed as combination of modular single-axis sliders. With the modular design, range of the possible applications can be

increased with adjustable operation spaces. Several example assembly configurations of modular single axis sliders are supplied. For the cases with vertical slider arrangement including the three-axis positioning system presented in this thesis, a counter balance subsystem is presented. Design processes of mechanical components of the three-axis slider system is explained.

Closed loop system setup illustration of a typical positioning device is given in Figure 1.1. As it can be observed from this figure, performance characteristics of positioning devices depend highly on the precision and resolution that can be obtained from the encoders. Yet, achievable resolution with decreasing the pitch of scale grating is limited by the available manufacturing technologies used for the optical encoders [16, 17]. For example, with the current available manufacturing technologies, commercially available linear optical encoders can have 0.512 micrometers scale grating in pitch satisfying 0.128 micrometers of optical resolution. Hence, in order to achieve high performance with the overall positioning system, it is crucial to increase the resolution of the encoders. Signal processing techniques for interpolation of the available encoder signals serves further improvement of the encoder resolution by deriving intermediate position values out of the original sinusoidal encoder signals.

In this thesis, a new adaptive approach to obtain high-resolution position information using the original encoder signals is presented. Our motivation here is to generate high-order quadrature sinusoids from the original encoder signals so that any deviations or distortions in these signals can be tolerated. Moreover, the approach is to be suitable for modular sliders in such a manner that application of the method on different encoders do not require any modifications in the algorithm. For this purpose, an adaptive signal conditioning step to obtain ideal sinusoids with quadrature phase difference is applied before the interpolation process. Then, mapping of the first-order signals to higher-order ones is accomplished by a quick-access look-up table. This table is generated offline by using the mathematical values of high-order sinusoids to increase the flexibility of the method for the application on modular slider systems. With the conversion of the high-order sinusoids to binary pulses, high-resolution position information is obtained. External validation of the presented encoder resolution improvement

method is accomplished using a laser vibrometer with known measurement resolution. Moreover, practical constraints limiting the application of the method is discussed. Performance of the method is examined by various experiments conducted on single, two and three axis positioning systems.

The remainder of this thesis is organized as follows. In Chapter 2, background information and previous works in the literature on high-precision positioning system design and encoder resolution improvement methods are reviewed. Chapter 3 presents design processes of the modular single-axis micro/nano-positioning device. Then, a specific three-axis configuration of single axis sliders is introduced. Chapter 4 proposes a new adaptive approach to obtain high-resolution position information out of the original encoder signals. Proposed signal correction and interpolation methods are discussed. Chapter 5 provides detailed information about the real-time implementation of encoder resolution improvement method using the Labview programming environment. In Chapter 6, validation of the encoder resolution improvement method is performed. Experiment results on the new method is also presented in this chapter. Effects of the presented method on positioning performance is examined. Conclusions and future work are discussed in Chapter 7.

Chapter 2

Background Information

In this thesis, development of a three axes high-precision positioning system and an encoder resolution improvement method proposed for this system is discussed. This chapter reviews the background information and previous work in these areas. For this purpose, firstly, current technologies on micro/nano-positioning systems is presented. Then, basic idea behind the encoder resolution improvement methods is explained and literature survey on this subject is introduced.

2.1 Micro/Nano-Positioning Systems

Micro/nano-scale applications require micro/nano-positioning devices with high precision and accuracy. High precision positioning devices are generally constructed as assembly of separately manufactured single axis slider systems [7, 5, 6]. Performance characteristics of these systems depend on positioning accuracy, maximum velocity and maximum acceleration that they can operate with acceptable performance based on the application. These characteristics are mostly determined by the actuator that gives motion to the slider. There is a strong relationship between properties of the actuator used and performance of the positioning system. Commonly used actuator types for positioning devices are ballscrew mechanisms [5, 11], piezoelectric actuators [8, 9, 10] and permanent magnet linear

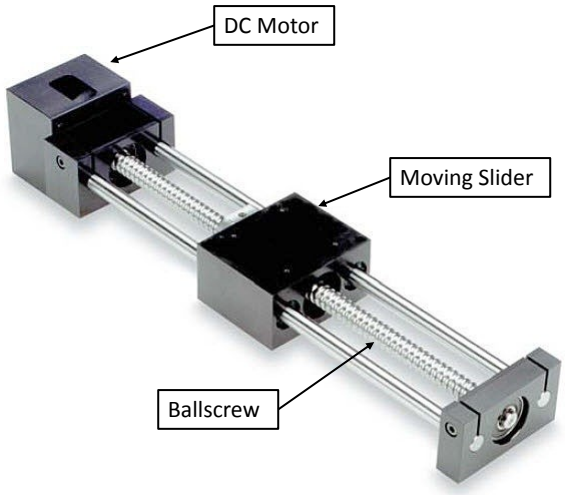

Figure 2.1: Ballscrew Mechanism [1]

motors [11, 18, 19, 20, 21, 12].

Ballscrew driven linear actuators are powered by a DC-motor and they can operate in long ranges. In these systems, a ballscrew is coupled with a DC-motor to convert the motor rotary motion into linear motion. An example ballscrew mechanism is given in Figure 2.1 showing the components of the system. As mentioned in literature, ballscrew mechanism driven linear stages have accuracy limitations due to backlash and wear of the mechanical components, and their acceleration and velocity capabilities are limited as a result of the ballscrew mechanism [19, 20, 22, 23, 24]. In this type of linear stages, one of the commonly used methods to calculate displacement of the slider is that angular position of the motor is measured and this measurement is simply multiplied by the pitch of the ballscrew. Due to the wear of the mechanical components in time, position, velocity and acceleration measurements obtained using this indirect measurement method may not be reliable [4, 5, 19].

Piezoelectric actuator (Figure 2.2) is another commonly used actuator type in precision positioning devices. Ceramic piezoelectric actuators convert voltage into displacement. Piezoelectric stage design includes flexures deflected by piezoelectric actuators. Although high accuracy and high precision values can be reached with piezoelectric stages, they cannot be used in many applications since they have limited work-space (less than 1 mm in each direction) and limited

Figure 2.2: Piezoelectric Actuator [2]

acceleration/velocity response [8, 4, 25].

With the recent commercial introduction of the linear motors, linear motor driven stages have been gaining popularity in precision engineering applications due to their superior characteristics [26]. A linear motor is an actuator that operates on a flat plane. Similar to working principle of DC motor, a linear motor converts electromagnetic force into mechanical motion. A linear motor is made of a coil and a magnet rail as shown in Figure 2.3. When current is applied on the coil, the magnetic force moves the motor on the magnet rail. The coil does not touch the magnet rail so that backlash or wear is not a concern. Moreover, nonlinearity due to contact mechanism is eliminated. Since linear motor driven stages do not require ballscrews, high acceleration and velocity values can be achieved [11, 27]. Furthermore, permanent magnet linear motors can operate in long ranges (typically greater than ten centimeters) compared to the piezoelectric motors. Position is measured directly on the stage with a linear encoder making the positioning extremely reliable. However, there are nonlinear disturbances in a permanent magnet linear motor due to force ripples that are caused by imperfections in the underlying components. These nonlinearities can be compensated through various control methods [18].

Another important component affecting the performance of a micro/nano-positioning device is the feedback sensor that supplies the position, velocity and acceleration information to the system. As feedback sensors, high-resolution sensors are used in micro/nano-positioning systems in order to satisfy high-precision.

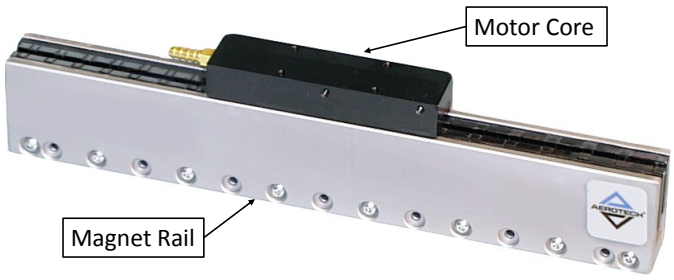

Figure 2.3: Permanent Magnet Linear Motor [3]

For this purpose, commonly used sensors are laser interferometers, capacitive sensors and optical encoders [12, 16, 17, 13]. Commercially available laser interferometers and capacitive sensors can reach up to sub-nanometer level measurement resolutions [28, 14]. However, their sensing range is very limited (usually smaller than one milimeter) [28, 14, 13]. On the other hand, measurement ranges of linear optical encoders may be around hundreds of milimeters. Yet, their resolutions are limited to micrometer level [15]. Maximum resolution value of a commercially available linear optical encoders is $0.128\mu m$ due to current manufacturing technologies. Hovewer, using signal processing techniques for interpolation of available encoder signals, nanometer level resolution can be obtained with linear optical encoders [16, 17, 29, 30]. Hence, linear optical encoders are advantageous over laser interferometers and capacitive sensors when long range of motion is main focus of interest.

2.2 Encoder Resolution Improvement Methods

As mentioned previously, precision and resolution of feedback sensor in the system have significant influence on performance characteristics of micro/nano-positioning devices. Therefore, it is important to have high resolution feedback sensors to obtain high positioning performance. However, available manufacturing technologies allow only micrometer level of scale grating for linear optical encoders (i.e. maximum $0.128\mu m$ optical resolution). Hence, further improvement in resolution of optical encoders is only possible with signal processing

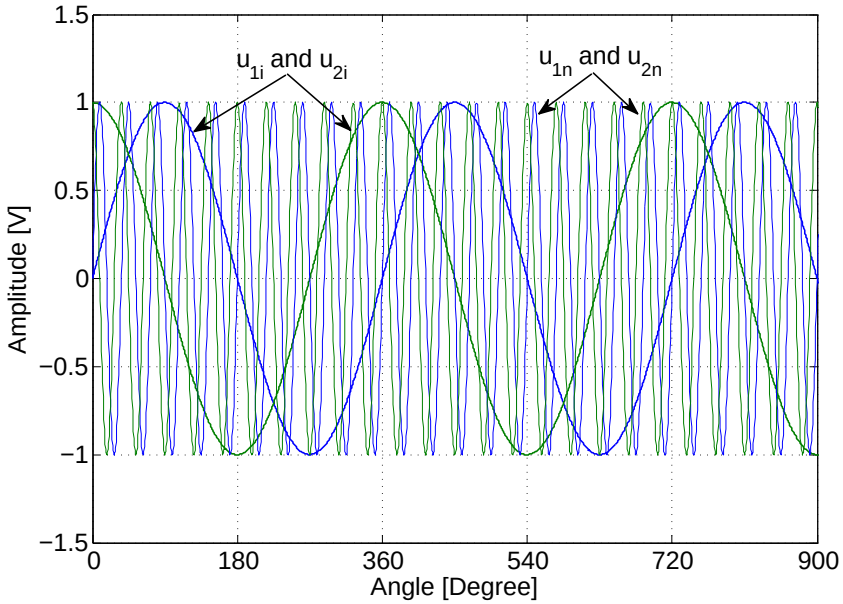

Figure 2.4: Ideal and Interpolated Encoder Signals

techniques. In order to increase the available resolution of an optical encoder, encoder signals should be interpolated to reach intermediate position values.

Basic idea behind an interpolation method is that high order sinusoidal signals can be generated from original first order analog encoder signals by using a suitable mapping function between them. Converting the calculated high order sinusoids to binary pulses and counting the zero-crossings, intermediate position information can be obtained. In Figure 2.4, an example interpolated signal pair is given with the ideal encoder signals to demonstrate the basic idea of an interpolation method. In this figure, u_{1n} and u_{2n} are high order signals (10^{th} order for this case) obtained as a result of interpolation process and u_{1i} and u_{2i} are ideal quadrature encoder signals.

Although it is possible to achieve high resolution values using various kinds of interpolation techniques, both hardware and software interpolation methods require ideal encoder signals with a quadrature phase difference between them. However, the encoder signals usually contain some noise and errors due to encoder scale manufacturing tolerances, assembly problems, operation environment conditions, and electrical grounding problems. Interpolation errors occur while

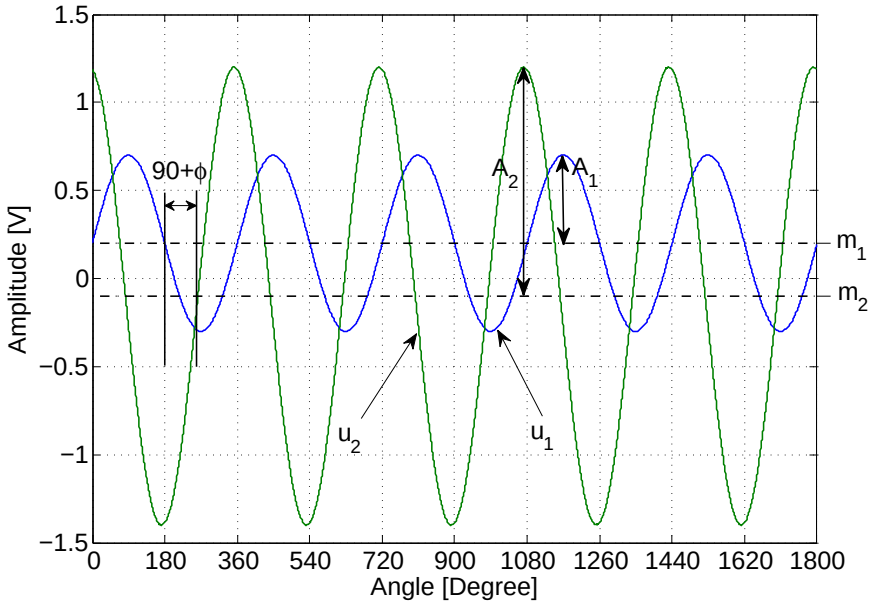

Figure 2.5: Exaggerated Illustration of Original Encoder Signals

extracting intermediate position information from the distorted pair of sinusoidal encoder signals. Therefore, these errors and noises have to be compensated before the interpolation method is applied. Common errors affecting the quadrature encoder signals are amplitude difference, mean offsets, and quadrature phase shift errors. In Figure 2.5, an exaggerated illustration of these errors are shown on an encoder signal pair, u_1 and u_2. In this figure, mean offsets are denoted as m_1 and m_2, amplitudes are A_1 and A_2 and ϕ is the phase shift error. For an ideal encoder signal pair, values of m_1 and m_2 should be $0V$, A_1 and A_2 should be $1V$ and ϕ should be $0degree$. Hence, the basic idea behind a correction method is to compensate these errors using mathematical relationship between distorted and ideal signal pair.

So far, many different approaches have been developed to correct the distorted encoder signals containing amplitude errors, mean offsets, and quadrature phase shift errors. The first introduced method was proposed by Heydemann [31]. In this method, errors in the encoder signal pairs are determined effectively using least squares minimization. Then, correction is done based on the calculated error values. Since the correction parameters are calculated offline, this method does not offer an effective compensation when the errors are changing dynamically

throughout the motion. Applications of this correction method can be found in [16] and [30]. In order to compensate the dynamic errors in encoder signals, several online compensation methods are developed. In [32], Balemi used gradient search method to calculate the correction parameters online, but performance of this method is not effective in low frequencies and noisy signals as mentioned in [33]. Another online error compensation method proposed in [17] corrects the sinusoidal signals obtained from a linear optical encoder by making use of an adaptive approach based on radial basis functions neural network. Then, authors use the similar procedure to increase the resolution of the encoder by mapping the original encoder signals to high-order sinusoids using another set of radial basis functions. Although high-resolutions can be achieved with this method, it requires a training period for every new encoder. Also, changes in the environmental conditions may require a new training period. Other interpolation methods also exist. In [34], Cheung proposed a sine-cosine interpolation method using logic gates and comparators. In [35], interpolation of encoder signals is accomplished by using digital signal processing (DSP) algorithms followed by digitization of sinusoidal encoder signals with analog-to digital converters (ADC). However, these interpolation approaches require external hardware such as high precision ADCs and DSPs to obtain high resolution from the encoder. Hence, their applicability to typical servo controllers with a digital incremental encoder interface is limited [17]. Another interpolation approach used so far is based on look-up tables. Tan et al. [16] obtained high-order sinusoids from original encoder signals using mathematical relationship between them. Then, they stored the values of high-order sinusoids in a look-up table. Using this table for online mapping of original encoder signals to higher-order ones, they managed to achieve intermediate position values leading high resolution values. Some other hardware and software based interpolation methods are also applied on magnetic encoders and resolver sensors [33, 36, 37].

Chapter 3

Design of Micro/Nano-Positioning Device

In this thesis, a specific design of a three-axis micro/nano-positioning device with $120mm\ x\ 120mm\ x\ 120mm$ operation space is the main focus of interest. However, this device is constructed by using three of the same modular single axis sliders perpendicular to each other. In this chapter, first, design of the modular single axis slider system is discussed in detail with its components and closed loop control setup. Improvements made on mechanical components during the design process of single axis slider are also summarized. Next, possible assembly configurations of designed modular single axis sliders are examined. Then, the specific three-axis configuration of sliders is introduced including the counter balance system, manufacturing and assembly tolerances of the system.

3.1 Modular Single-Axis Slider System

Our three-axis positioning system will be composed of three modular single axis stages assembled perpendicularly as shown in Figure 3.1. As a first step to develop this system, a modular linear slider that can achieve micro/nano-meter level positioning over $120mm$ operation range is built. In Figure 3.2, a 3D model

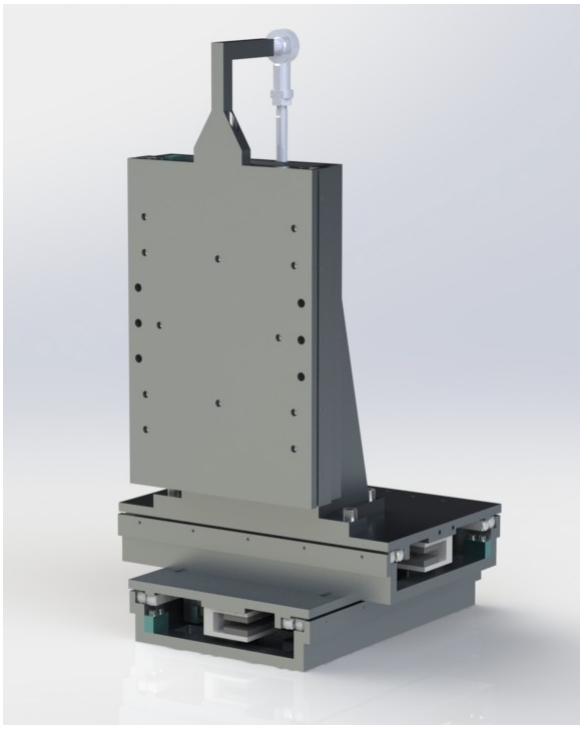

Figure 3.1: 3D Drawing of Three-Axis Positioning System

of designed single axis linear slider is given. While designing this slider system, components are chosen elaborately to accomplish their specific purpose for micro/nano-positioning tasks. In this section, mechanical and electrical components of the single axis slider system is given. Control setup of the closed loop system is also introduced. Then, details of design improvements of mechanical components are explained with reasoning.

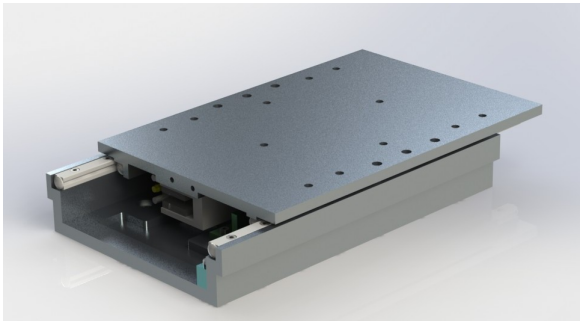

Figure 3.2: 3D Drawing of Single-Axis Slider

3.1.1 Components and Control Setup

Performance of a micro/nano positioning device can be evaluated by its working range, maximum velocity and acceleration, positioning resolution and positioning accuracy values. Components of the single axis slider presented in this thesis are chosen considering these performance characteristics. Moreover, modularity is another concern while designing the mechanical components of the slider.

As illustrated in Figure 3.3 and Figure 3.4, modular single axis slider is designed with a stationary base and a moving slider that are connected to each other via cross-roller linear bearings from THK. The stage is actuated by a brushless permanent magnet linear motor from Aerotech Inc. (BLMUC-95 and MTUC-224) whereas the position feedback is taken from an optical linear incremental encoder from Heidenhain Corp. (LIP 481R). In addition to linear motor, optical encoder and linear bearings, eight mechanical components are designed and manufactured for the modular single axis slider.

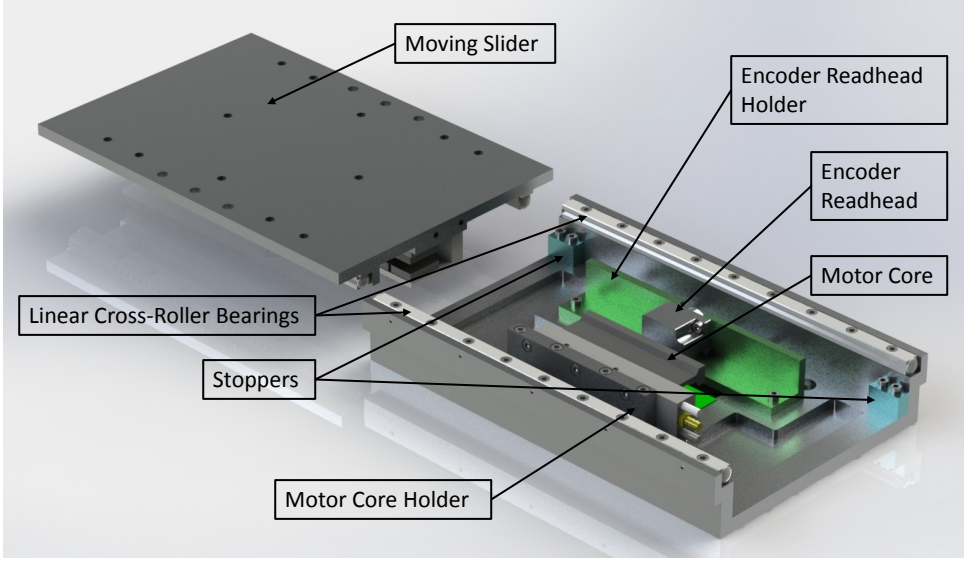

Figure 3.3: Top View of the Designed Single Axis Slider

In design of the single axis slider, linear bearings are chosen to satisfy linear motion of the sliding part with minimum friction. Cross-roller bearings are used to carry both vertical and horizontal loads effectively. In order to satisfy high

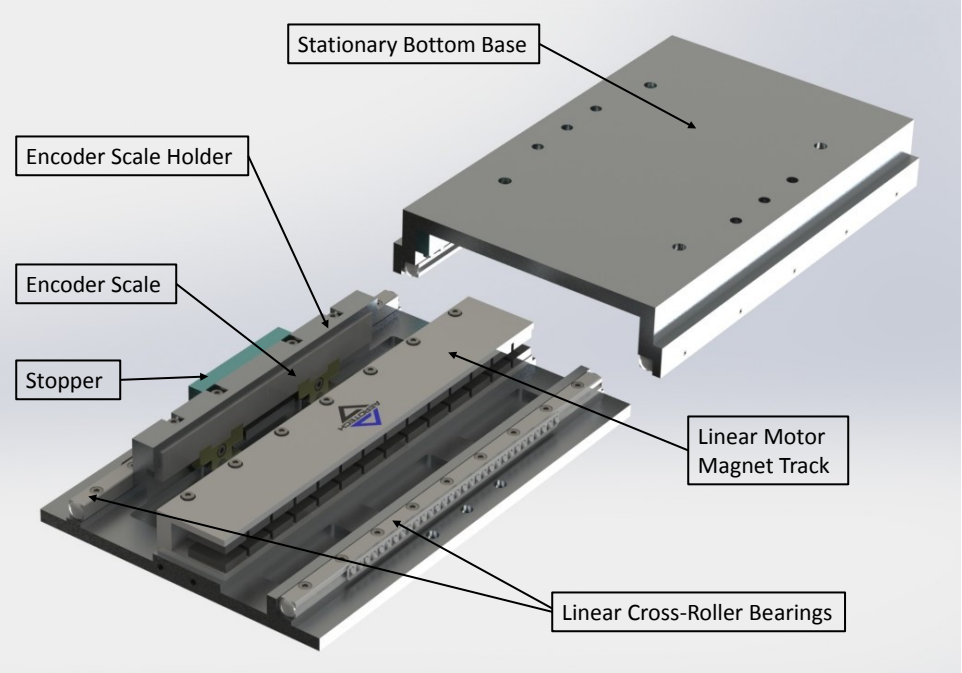

Figure 3.4: Bottom View of the Designed Single Axis Slider

precision motion, VR model low-friction, high-accuracy, precision roller bearings [38] are preferred.

As the actuator, permanent magnet linear motor is chosen due to its outstanding characteristics in precision positioning applications. The most important feature of this type of actuator is that long ranges (more than $100mm$) can be traveled with high velocity and acceleration. The chosen linear motor, BLMUC-95, is a very compact linear motor with $52.0mm\ x\ 20.8mm$ cross section and $224mm$ track length. This feature makes it suitable for compact systems. In order to satisfy desired $120mm$ motion, track length is chosen as $224mm$ since linear motors can operate effectively only when the motor coil is inside of the magnet track completely. As mentioned in [3], backlash, windup, wear and maintenance issues associated with ball screws, belts, and rack and pinions are eliminated by non-contact design of the motor. Moreover, more than $25N$ force can be generated by this motor. Some important specifications of the linear motor used in the single axis slider system is given in Table 3.1.

In the single axis slider design, position is measured directly on the stage with

Table 3.1: Specifications of BLMUC-95 Linear Motor

Specifications	**Units**	**BLMUC-95**
Continuous Force 1.4 bar	N	40.5
Continuous Force, No Air	N	23.0
Peak Force	N	161.9
Coil Weight	kg	0.12
Coil Length	mm	96
Magnet Track Weight	kg/m	3.33

an optical linear incremental encoder (LIP 481R) so that positioning measurements become extremely reliable. This encoder has $4\mu m$ scale grating in pitch satisfying $1\mu m$ original measurement resolution. However, this resolution is increased up to $10nm$ using a new encoder interpolation technique presented in Chapter 4. As described in [15], the readhead and scale of the optical encoder are assembled on the system so that the distance between them is approximately $0.6mm$ for effective measurements with low noise levels. In order to satisfy this assembly requirement, a specific plastic sheet with $0.6mm$ thickness is placed between the readhead and the scale so that mounting screws can be tighten in correct positions.

As mentioned previously, eight mechanical components are designed and manufactured for the single axis slider. These parts are stationary bottom base, moving slider, stopper parts, motor core holder, encoder readhead holder and encoder scale holder. All of these parts can be seen in Figure 3.3 and Figure 3.4. While designing these parts, the main concerns are ease of assembly, modularity and compactness. Moreover, geometrical properties of these parts are designed to keep their rigidity during the manufacturing processes. For modularity purposes, each part is designed so that a single axis slider can be assembled on another one in various configurations to build single, two or three axis systems for different

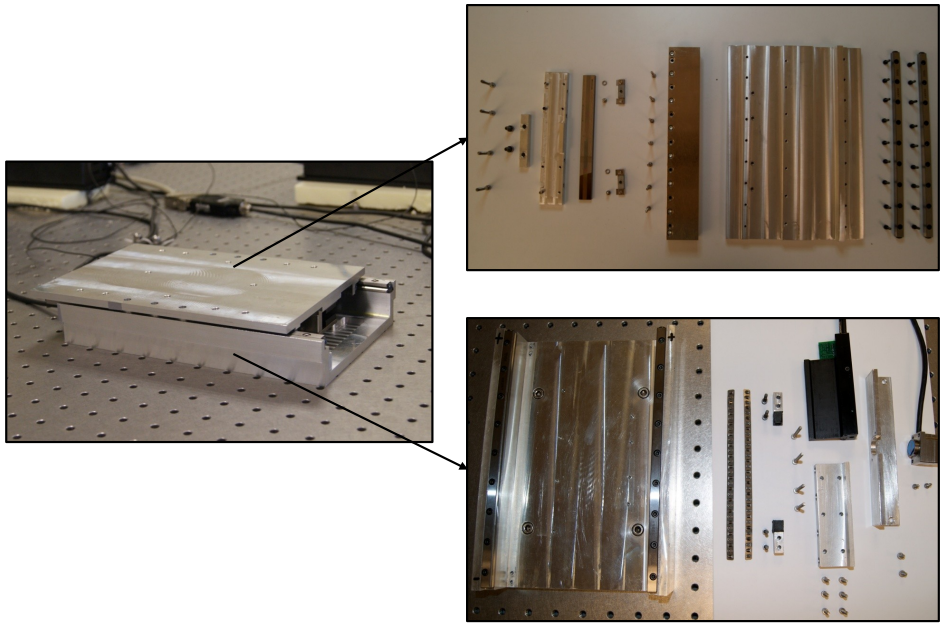

Figure 3.5: Single Axis Slider with its Components

applications. Here, any of the configurations can be built without making any modifications in the single axis slider. In Figure 3.5, designed single axis slider is given with all of its components.

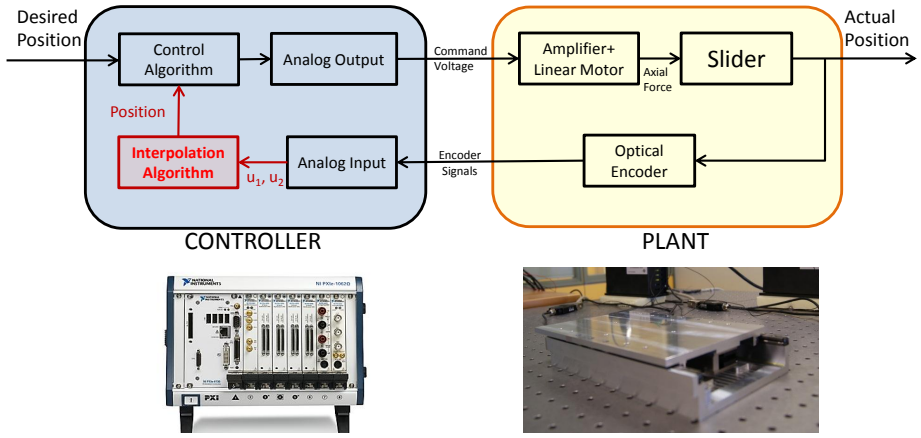

Figure 3.6: Closed Loop Control System Setup of the Single Axis Slider

In addition to a suitable mechanical design for micro/nano-positioning applications, an appropriate control setup is required to control the single axis slider system with high precision. Closed loop configuration of the control system for

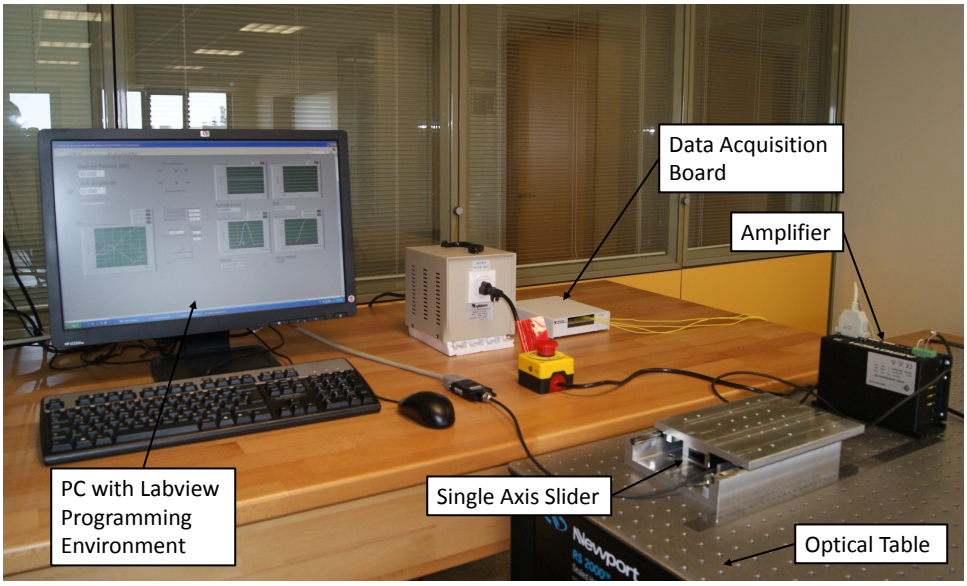

Figure 3.7: Photograph of Testbed for the Single Axis Slider

single axis slider is given in Figure 3.6. As it is shown in this figure, a controller and an amplifier is required in the control system. In our system, control algorithm is developed on a PC using NI Labview programming environment. Several control schemes are used to control the system including the basic PID control and more complex control techniques such as iterative learning [39], model reference adaptive control. A standard current commanded six-point commutation amplifier from Aerotech Inc. (BA20) is used as an amplifier. In this setup, liner optical encoder data is acquired using an analog data acquisition card attached on the PC. Same data acquisition card is used to send control inputs to the system. All of these components can also be seen in the testbed photograph for single axis slider in Figure 3.7.

3.1.2 Design Improvements of Mechanical Components

During design process of the single axis slider system, several improvements are made on the mechanical components to be manufactured. These improvements are made to increase the performance of the system, to make the assembly easier and to increase the rigidity and modularity of the slider. In Figure 3.8, top view

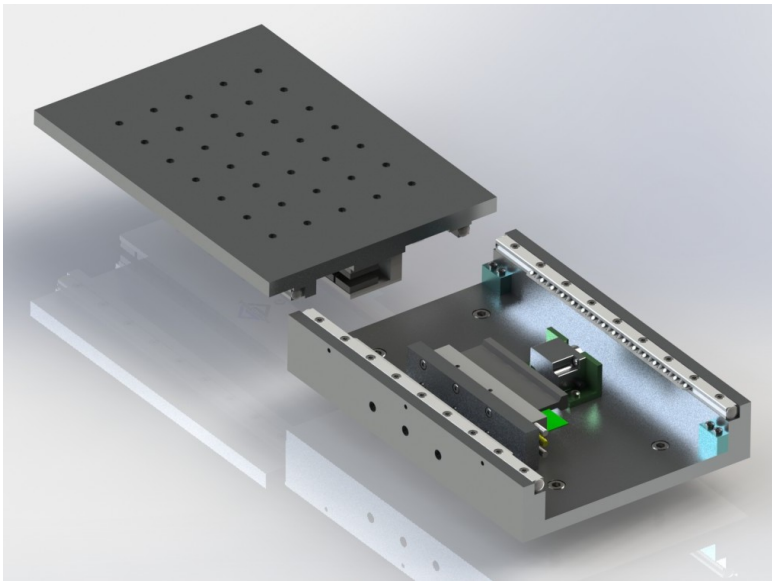

(a)

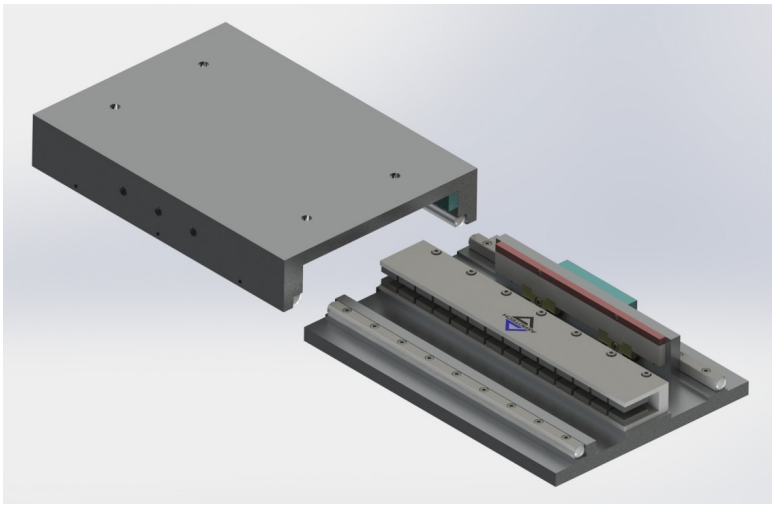

(b)

Figure 3.8: (a) Top and (b) Bottom View of the Previous Single Axis Slider Design

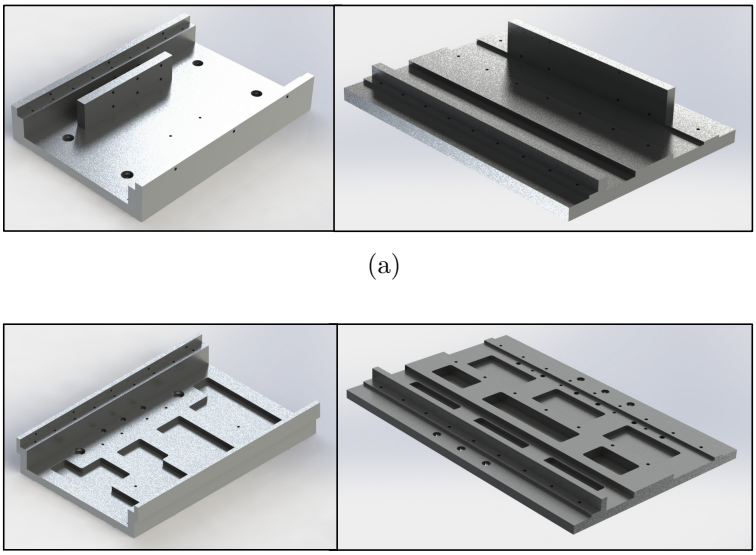

(a)

(b)

Figure 3.9: Moving Sliders and Stationary Bottom Bases of (a) Previous and (b) New Single Axis Slider Designs

and bottom view of the first design for single axis slider is given to illustrate the modifications on the components clearly.

One of the main modifications is accomplished on moving slider and stationary bottom base to decrease the system weight. This process was required to increase the positioning performance of the system. For this purpose, thickness of these parts are reduced and partial removal of material is done in specific areas. These areas are determined considering the positions of mounting screws so that the rigidity of the component is not affected. Moreover, number of mounting screw holes on top of moving sliders are reduced without changing modularity characteristics of the slider. Another major change in moving slider and stationary bottom base is that encoder scale holder and motor holder are manufactured as separate parts in the new design. Reason of this modification is to make the assembly and manufacturing easier. In Figure 3.9, previous and new moving sliders and stationary bottom bases are given to show the main modifications. As it can be seen in this figure, there are three holes at each side of new moving slider design and stationary bases. These holes are added in order to assemble linear

(a) (b)

Figure 3.10: (a) Previous and (b) New Scale Holder Designs

bearings easily. Using these holes, fine adjustments of three mounting screws at the middle of linear bearings can be done even after whole slider system is assembled together.

Another important modification is made on encoder scale holder. In previous designs, encoder scale is supported by a simple beam attached under it and sides of the encoder scale were open as shown in Figure 3.10a. Hence, assembly of the encoder scale to the desired position was not possible. For this purpose, in the most recent design, encoder scale holder is modified as shown in Figure 3.10b. In this design, the support beam is removed and a single piece scale holder is designed so that the sides are closed and encoder scale can only fit to the correct place. There is also a screw on the one side of the scale holder to tighten up the scale.

Since one of the stopper parts is attached to the encoder scale holder, screws between stopper and encoder scale holder and screws between scale holder and moving slider may exposed to sudden forces if any uncontrolled motion happens. In order to eliminate this risk, some steel pins with diameter of $4mm$ and $5mm$ are placed in these critical areas to carry those forces. For these pins, tight tolerance is used. Positions of the pins are shown in Figure 3.11.

The last major change applied on the single axis slider is about the design of encoder readhead holder. In the first design, since length of the encoder readhead holder is small as shown in Figure 3.8a, it is almost impossible to adjust $0.6mm$ distance between the encoder readhead and the scale without disassembling the moving slider from the stationary base. In order to overcome this problem, length of the readhead holder is increased so that the mounting screws of the holder can

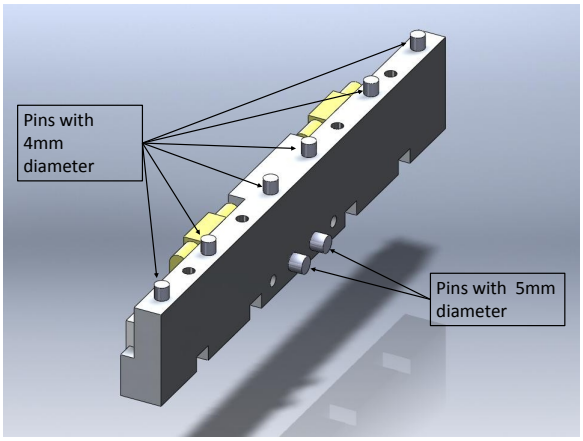

Figure 3.11: Safety Pins on Encoder Scale Holder

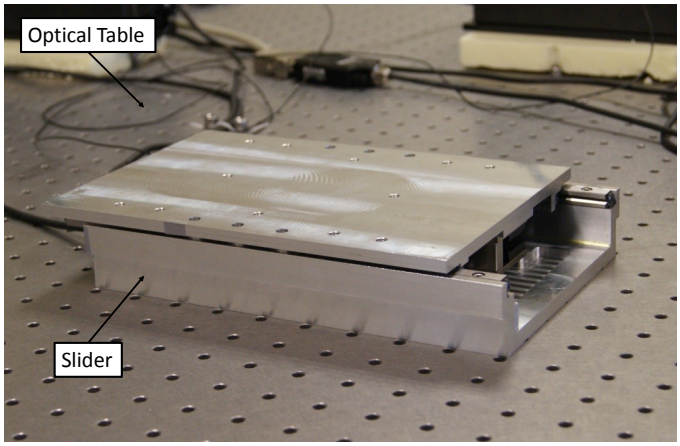

Figure 3.12: Single Axis Slider

be reached when the moving slider part is at one of its utmost positions. Final design of the encoder readhead holder can be seen in Figure 3.3.

After the mentioned design improvement processes, manufacturing and assembly of single axis slider is accomplished for the final design. A picture showing the modular single axis slider is given in Figure 3.12. This design is also used for two and three axis configurations in this thesis.

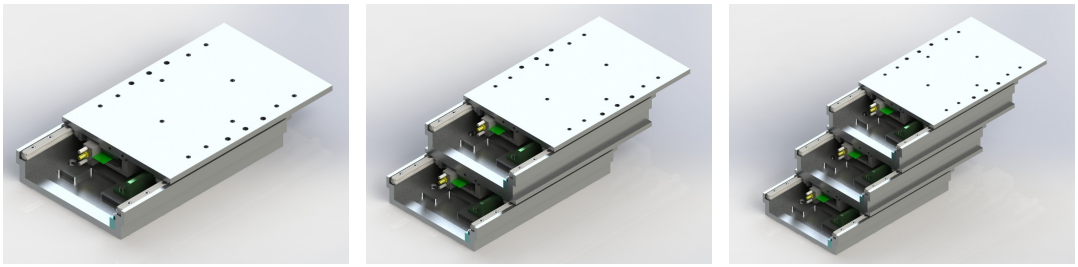

(a) (b) (c)

Figure 3.13: Example Single Axis Assembly Configurations with a One, (b) Two and (c) Three Sliders

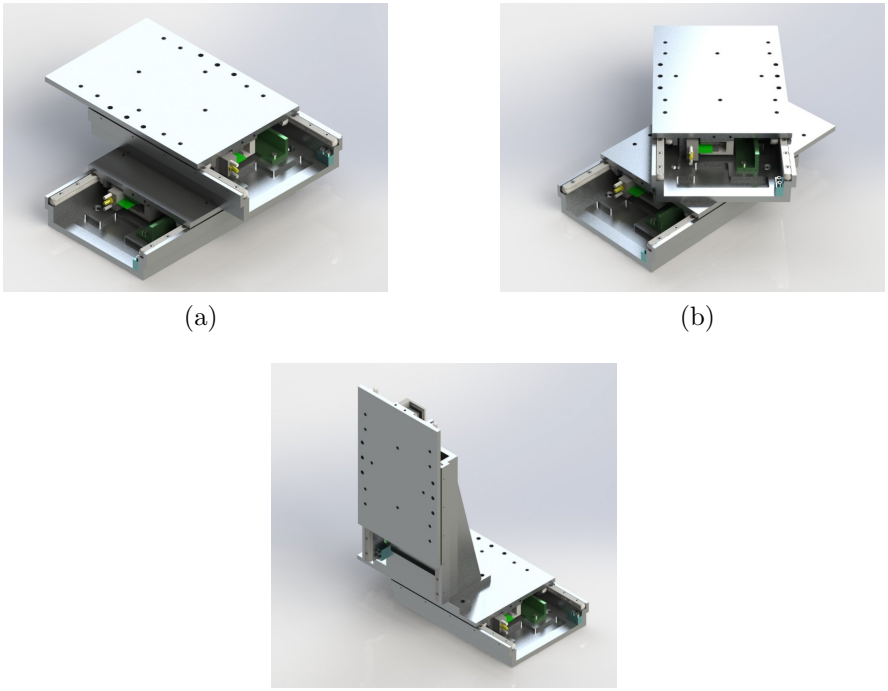

(a) (b)

(c)

Figure 3.14: Example Two Axis Assembly Configurations Using Two Sliders in a X-Y (b) Oblique X-Y and (c) X-Z Arrangements

3.2 Assembly Configurations of Modular Slider

As mentioned in previous sections, modularity was one of the main concerns while designing the single axis slider. In this section, modularity feature of designed single axis slider system is illustrated. Several possible configurations are given for single, two and three axis systems.

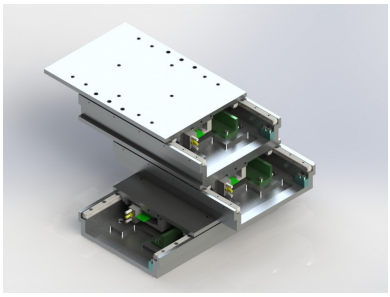

(a)

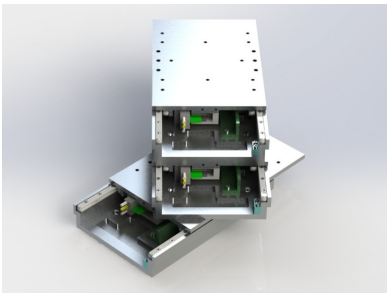

(b)

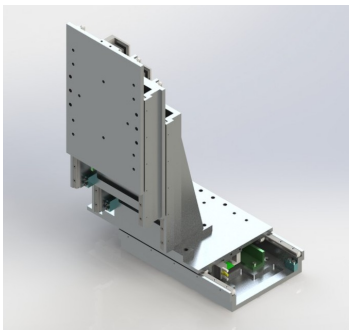

(c)

Figure 3.15: Example Two Axis Assembly Configurations Using Three Sliders in a X-Y (b) Oblique X-Y and (c) X-Z Arrangements

Due to the modularity property of the designed single axis slider, couple of them can be assembled to built a single, two or three axis positioning system for different applications. By assembling the single axis sliders in different forms, systems with various reachable operation areas can be obtained for many specific applications. In Figure 3.13, Figure 3.14, Figure 3.15 and Figure 3.16, several possible assembly configurations for single, two and three axis systems are given. In all of these design, maximum three number of sliders are used. However, it is possible to built different systems by assembling more than three single axis sliders to satisfy specific applications. As it can be observed from Figure

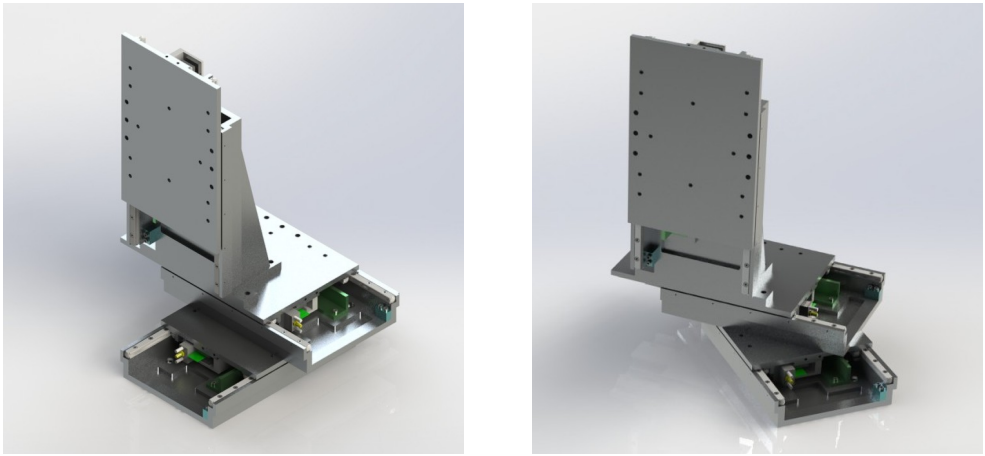

(a) (b)

Figure 3.16: Example Three Axis Assembly Configurations Using Three Sliders in a X-Y-Z (b) Oblique X-Y-Z Arrangements

3.13, range of the system increases to its triple value with the addition of two other sliders. Similarly, reachable operation areas of the two axis systems shown in Figure 3.14 and Figure 3.15 increase as the number of sliders are increased. Moreover, it is possible to adjust the limits of the reachable operation area in each axis by assembling one or couple of sliders obliquely. By adjusting the angle of the oblique sliders, a rectangular working area can be obtained instead of a square one.

As it can be observed from Figure 3.14b, Figure 3.15b and Figure 3.16, configurations including vertical arrangements of single axis sliders, a support system is required to keep the slider in vertical position. An example support system design including a compensation system for the weight of vertical slider is explained in Section 3.3.1.

Although there are various possible assembly configurations as summarized in this section, the systems used in real time experiments are the ones shown in Figure 3.13a, Figure 3.14a and Figure 3.16a. Photographs of manufactured single axis slider and two axis slider system are given in Figure 3.12 and Figure 3.17, respectively. Details of three-axis slider system is given in Section 3.3.

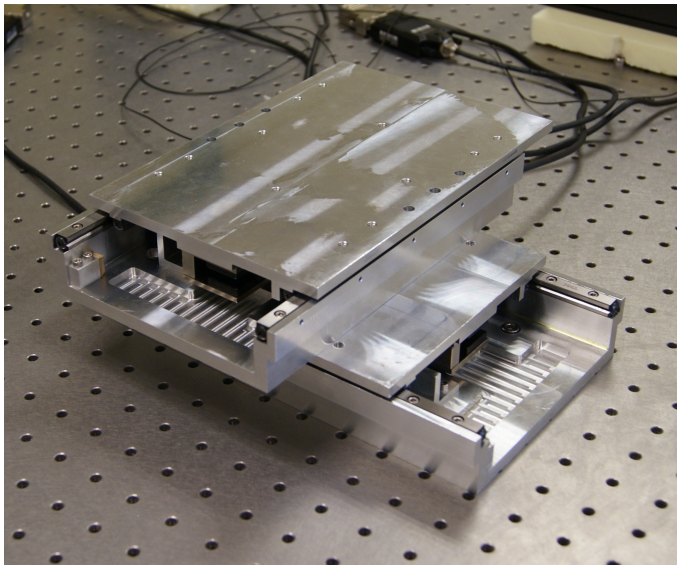

Figure 3.17: Two Axis Slider System

3.3 Three-Axis Slider System

In Figure 3.18, manufactured three axis micro/nano-positioning device is shown. As mentioned previously, this specific design is composed of three of the same modular single axis sliders that are assembled perpendicular to each other. For the vertical axis, a support system is used to keep the slider in vertical position and to compensate the weight of the moving part. This system is called as counter-balance system in this thesis. In this section, details of designed three-axis micro/nano-positioning device is discussed. First, counter balance subsystem is presented. Then, details on manufacturing tolerances and assembly technique are summarized.

3.3.1 Counter Balance Subsystem

A counter balance subsystem is used in three axis positioning system for assembly of third slider. This subsystem is designed as an adapter for the single axis slider to be used in vertical position. It is composed of two main parts: an L shaped beam structure and an air piston. The purpose of the L shaped beam is to

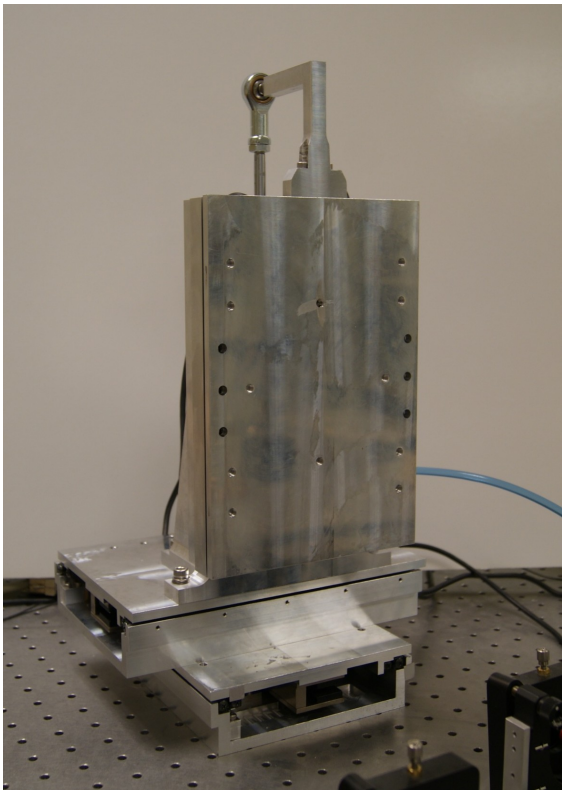

Figure 3.18: Three Axis Micro/Nano-Positioning System

support the slider in vertical position. On the other hand, air piston is used to compensate the weight of the sliding part so that similar control inputs can be used in both directions in vertical for high precision positioning. In addition to these main parts, a connector, a spherical joint and a pressure regulator are also used in counter balance system. The connector is used to connect the moving slider of vertical stage to the air piston via a spherical joint. On the other hand, pressure regulator is used to adjust the air pressure going to the air piston.

In Figure 3.19, counter balance subsystem used in three-axis positioning system is shown. In this subsystem, air pressure coming from the common source to the piston is adjusted using an analog pressure regulator. Hence, when a part is assembled on the vertical slider for a specific application, difference in the weight of the vertical sliding part can be compensated by using the regulator to adjust the pressure coming to the piston. In the three axis positioning system, when

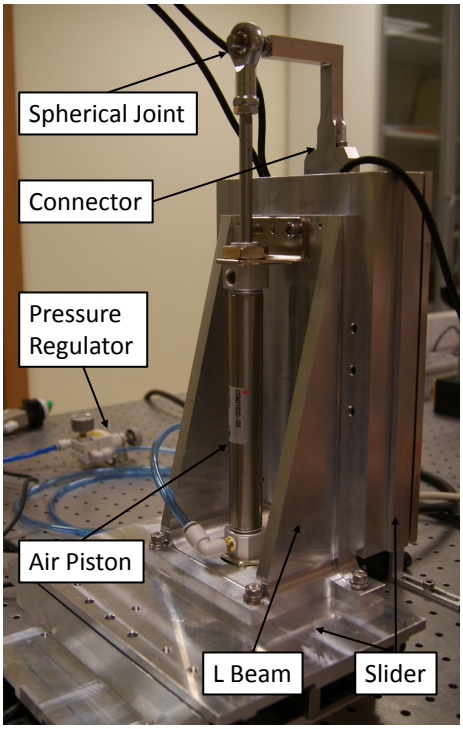

Figure 3.19: Counter Balance Subsystem

there is no additional part is assembled, 6 *bar* of pressure coming from the common source is reduced to approximately 1 *bar* using the pressure regulator and fed into the air piston to compensate the weight of the moving slider in vertical axis.

3.3.2 Manufacturing and Assembly Tolerances

Tolerances are crucial while designing, manufacturing and assembling a system to work in nanometer level precision. In order to obtain maximum performance from actuator and sensor units, manufacturing and assembly tolerance values should be determined carefully for the assembly regions of these parts.

A 3D drawing of the slider is given in Figure 3.20 showing the tolerance critical sections. As it can be observed in this figure, the important sections in terms of tolerances are the ones that encoder and linear motor are attached to the system. Moreover, top and bottom surfaces of the slider are also important in terms of

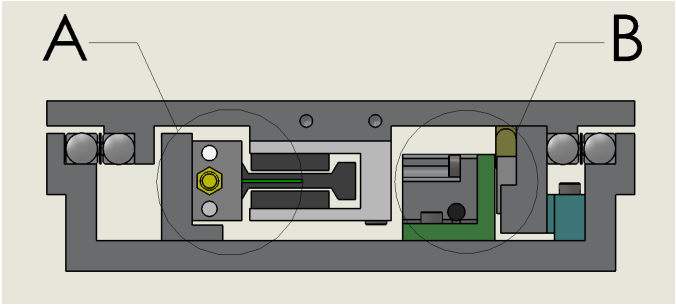

(a)

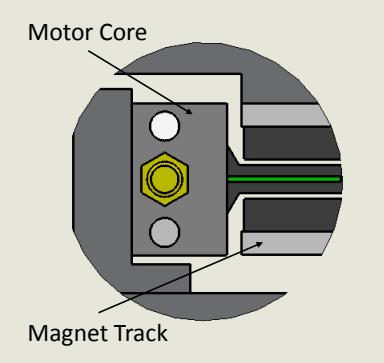

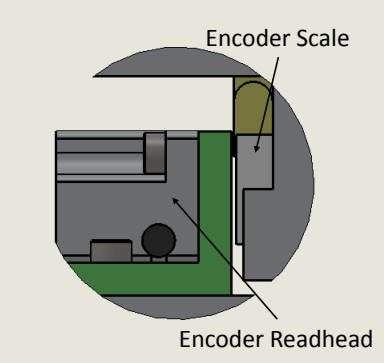

(b) (c)

Figure 3.20: (a) Tolerance Critical Sections of Single Axis Slider with Detail Views of (b) Section A and (c) Section B

their flatness and surface roughness values since these surfaces are the contact regions while mounting the slider on the optical table or another slider.

Figure 3.20c shows the assembly region of the encoder readhead and the scale. In order to obtain measurements with minimum error from the encoder, they should be assembled according to some predefined specifications. For this purpose, tolerances for the regions where the encoder readhead and the scale attached are determined according to the instructions supplied by the encoder manufacturer [15]. Therefore, surface flatness tolerance is chosen to be $0.01mm$ for these regions. Moreover, distance between the encoder readhead and the scale is to be $0.6mm$, hence tolerance for this distance is determined as $0.02mm$ to be satisfied during the assembling process. Tolerances for positions of screw holes that the encoder head and the scale are to be attached are chosen as $0.05mm$ in each direction.

Similar to encoder assembly, flatness of the surfaces that the linear motor is attached is critical. Flatness tolerance of the assembly surfaces shown in Figure 3.20b is chosen to be $0.01mm$. Position of the motor is also be arranged by using $0.05mm$ tolerance in the locations of the mounting screw holes.

Flatness properties of the top and bottom surfaces of single axis sliders are also important for them to be assembled on the optical table or to be assembled together to built three axis positioning system with nanometer level positioning precision. Therefore, as in encoder and linear motor assembly, geometric tolerance for flatness of these surfaces is chosen to be $0.01mm$.

Chapter 4

Encoder Resolution Improvement Method

In this thesis, presented single axis slider system includes a linear incremental optical encoder as a feedback sensor to obtain position information. However, measurement resolution of the encoder used in the system is $1\mu m$ since the scale grating is $4\mu m$ in pitch. Precision positioning in sub-micrometer level is impossible using this encoder. Hence, in order to achieve nanometer level positioning performance with overall system, it is crucial to increase the resolution of the encoder used. Signal processing techniques for the interpolation of the available encoder signals serves further improvement of the encoder resolution by deriving intermediate position values out of the original encoder signals.

In this chapter, a new adaptive approach to obtain high-resolution position information out of the original encoder signals is presented. First, the overview of the approach is given to give the basic idea behind it. Next, the adaptive encoder signal correction technique used before the interpolation process is presented with the mathematical foundation. Then, signal interpolation method is discussed in detail. Generation of binary pulses from the interpolated signals and deriving position information using these binary pulses are explained. Lastly, practical constraints that limit the application of this approach is summarized.

4.1 Overview of the Proposed Approach

As briefly discussed in [29], our motivation in this approach is to generate high-order quadrature sinusoids from the original encoder signals so that any deviations or distortions in these signals can be tolerated. For this purpose, an adaptive signal conditioning step to obtain ideal sunusoids with quadrature phase difference is applied before the interpolation process. Then, mapping of the first-order signals to higher-order ones is accomplished by a quick access look-up table. With the conversion of the higher-order sinusoids to binary pulses, high-resolution position information is obtained.

Proposed method features two main steps: (1) correction of signal errors and (2) interpolation of corrected signals. For the correction step, an adaptive correction method is adopted to compensate the encoder signal errors including amplitude difference, mean offsets, and quadrature phase shift errors. Adaptation is performed by the recursive least squares (RLS) with exponential forgetting and resetting. The need for adopting an adaptive correction technique is due to the dynamic characteristics of the errors as well as the applicability on different encoders without any modification.

For high precision positioning applications, assembly and alignment of the encoder is very important to attain required accuracy and precision. However, for closed systems or long range positioning systems, it may not be possible to align the encoder to obtain perfect quadrature signals. Characteristics of the resulting signal may change through the motion. Hence, adaptive approach used in this section is more suitable for the systems where the signal errors change dynamically. Moreover, adaptive characteristics of the correction step makes the method applicable to different encoders without requiring any modification in the algorithm. Due to the adaptive approach in the correction method, different error characteristics of different encoders can be compensated without changing any parameter in the algorithm.

In the second step of the proposed method, interpolation of the corrected signals is satisfied by a look-up table based approach. In this approach, the basic

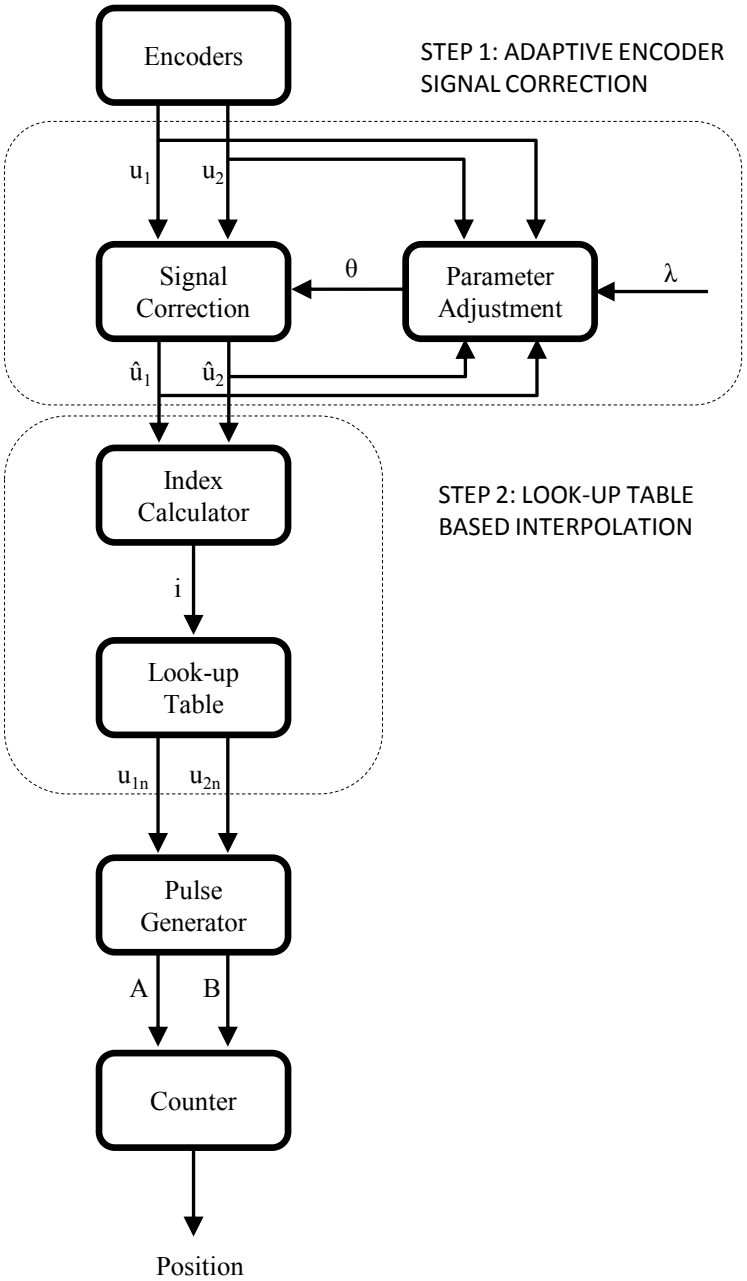

Figure 4.1: General Flow Diagram of the Proposed Approach

idea is to obtain high-order sinusoids from original encoder signals by mapping the original signals to high-order ones online with the help of a quick access look-up table. Since the look-up table is formed offline, computational effort is considerably less compared to the previously mentioned online interpolation methods. At the end of the interpolation stage, position information can be derived from conversion of the high-order sinusoids to binary pulses. This conversion is also implemented on the software hence it is accomplished without using any additional hardware such as high precision ADCs.

An overall flow diagram for the proposed approach is shown in Figure 4.1. In this figure, signal correction and interpolation steps are labeled as Step 1 and Step 2, respectively. The correction step takes the encoder signals u_1 and u_2 and generates signals $\hat{u}_1$ and $\hat{u}_2$ as corrected quadrature signals. In order to compensate the errors in u_1 and u_2, a set of correction parameters $\boldsymbol{\theta}$ is calculated using RLS with exponential forgetting and resetting in the parameter adjustment stage. Here, our parameter adjustment rule uses the current encoder signals u_1 and u_2 and corrected signals $\hat{u}_1$ and $\hat{u}_2$ from previous iteration. λ is the forgetting factor or discounting factor. When the correction step is completed, index calculator generates index, i, for signals to obtain corresponding high-order sinusoid values, u_{1n} and u_{2n}, from the look-up table. The look-up table is constructed using the correct values of high-order sinusoids since the corrected signals coming from the Step 1 are calculated with sufficient precision through the adaptive correction scheme. Therefore, the look-up table can be generated offline without requiring high computational effort. Using high-order sinusoids, pulse generator generates quadrature binary pulses A and B. As mentioned previously, this process is performed in the software part without requiring high-precision ADCs. Finally, position value is calculated by detecting zero crossings of high-resolution binary pulses.

4.2 Adaptive Encoder Signal Correction (Step 1)

Before the interpolation stage, it is crucial to correct the errors in the original encoder signals to prevent high interpolation errors. Common errors affecting the quadrature encoder signals are the amplitude difference, the mean offsets and the quadrature phase shift errors. In Figure 2.5, an exaggerated illustration of these errors are given. In this figure, mean offsets are denoted as m_1 and m_2, amplitudes are A_1 and A_2 and ϕ is the phase shift error.

In this section, an adaptive approach is used to correct the errors. In some applications, it is possible to have similar error characteristics throughout the motion. In these cases, the error can be compensated using offline correction methods given in [16] and [31]. On the other hand, in some cases where the encoder alignment cannot be performed effectively or where the systems have long range of movement track, the errors change throughout the motion. For such cases, adaptive approaches may be adopted to track the errors better in order to obtain high-resolution. Moreover, with an adaptive approach, applicability of the method on different encoders with different error characteristics can be satisfied without requiring any modification in the algorithm. For this purpose, RLS with exponential forgetting and resetting method is developed to adjust correction parameters online.

In order to develop the mathematical foundation (i.e. (4.1)-(4.15)) for our proposed method, we will start with the formulation given in [31].

An ideal set of quadrature encoder signals with amplitude of A, u_{1i} and u_{2i}, can be expressed as

$$\begin{aligned} u_{1i} &= A\cos\alpha \\ u_{2i} &= A\sin\alpha \end{aligned} \tag{4.1}$$

where α is the instantaneous phase of the signals with phase difference of $\pi/2$.

Relation between real (u_1 and u_2) and ideal encoder signals (u_{1i} and u_{2i}) can be written as

$$\begin{aligned} u_1 &= u_{1i} + m_1 \\ u_2 &= \frac{1}{R}(A_1 \cos(\alpha - \phi)) + m_2 \end{aligned} \tag{4.2}$$

where m_1 and m_2 are mean offset values and ϕ is the quadrature phase shift error. In (4.2), R is the gain ratio (A_1/A_2) where A_1 and A_2 are amplitudes of actual encoder signals. Using (4.1) and (4.2), a conventional least squares formulation can be obtained as shown in (4.3) and (4.4).

$$\theta_1 {u_1}^2 + \theta_2 {u_2}^2 + \theta_3 u_1 u_2 + \theta_4 u_1 + \theta_5 u_2 = 1 \tag{4.3}$$

where

$$\begin{aligned} \theta_1 &= (A_1^2 \cos^2\phi - m_1^2 - R^2 m_2^2 - 2Rm_1 m_2 \sin\phi)^{-1} \\ \theta_2 &= \theta_1^2 R^2 \\ \theta_3 &= 2\theta_1 R \sin\phi \\ \theta_4 &= -2\theta_1(m_1 + Rm_2 \sin\phi) \\ \theta_5 &= -2\theta_1 R(Rm_2 + m_1 \sin\phi) \end{aligned} \tag{4.4}$$

It is possible to calculate θ_i ($i = 1, 2, , 5$) constants offline using least squares. In order to use a Recursive Least Squares (RLS) approach with exponential forgetting, (4.3) can be re-written as shown in (4.5).

$$\begin{aligned} &\varphi_1(t)\theta_1(t) + \varphi_2(t)\theta_2(t) + \varphi_3(t)\theta_3(t) + \varphi_4(t)\theta_4(t) \\ &+ \varphi_5(t)\theta_5(t) = 1 \\ &or \\ &\boldsymbol{\varphi}^T(t)\boldsymbol{\theta}(t) = 1 \end{aligned} \tag{4.5}$$

where superscript T denotes transpose of a matrix, t is time index, $\theta_i's$ are

parameters to be determined and $\varphi_i's$ are known functions depending on actual encoder signal values. Then, the parameter update and regressor vectors given in (4.6) are obtained.

$$\begin{aligned} \boldsymbol{\varphi}^T(t) &= [u_1^2(t), u_2^2(t), u_1(t)u_2(t), u_1(t), u_2(t)] \\ \boldsymbol{\theta}(t) &= [\theta_1(t), \theta_2(t), \theta_3(t), \theta_4(t), \theta_5(t)]^T \end{aligned} \tag{4.6}$$

The objective of a RLS with exponential forgetting and resetting algorithm is to determine the parameters so that (4.5) is satisfied with minimum possible error. For this purpose, a loss function given in (4.7) is determined so that the chosen $\boldsymbol{\theta}$ should minimize its value.

$$V(\boldsymbol{\theta}, t) = \frac{1}{2}\sum_{k=1}^{t} \lambda^{t-k}(1 - \boldsymbol{\varphi}^T(k)\boldsymbol{\theta})^2 \tag{4.7}$$

where k is index and λ is forgetting factor such that $0 < \lambda \leq 1$. By adjusting the value of λ, contribution of old data to loss function is controlled so that most recent data is given unit weight whereas old data is weighted by λ^s, where s is number of time intervals elapsed from the old data.

Then, the recursive parameter adjustment law can be obtained as follows:

$$\begin{aligned} \boldsymbol{\theta}(t) &= \boldsymbol{\theta}(t-1) + \boldsymbol{K}(t)(1 - \boldsymbol{\varphi}^T(t)\boldsymbol{\theta}(t-1)) \\ \boldsymbol{K}(t) &= \boldsymbol{P}(t-1)\boldsymbol{\varphi}(t)(\lambda + \boldsymbol{\varphi}^T(t)\boldsymbol{P}(t-1)\boldsymbol{\varphi}(t))^{-1} \\ \boldsymbol{P}(t) &= (\boldsymbol{I} - \boldsymbol{K}(t)\boldsymbol{\varphi}^T(t))\boldsymbol{P}(t-1)/\lambda \end{aligned} \tag{4.8}$$

where $\boldsymbol{I}$ is identity matrix and $\boldsymbol{P}$ is a non-singular matrix which can be chosen as $\boldsymbol{P} = \kappa\boldsymbol{I}$, κ is a large number.

For simplicity, time index t will be dropped from the equations from this point forward, although each correction parameter is time-varying. For calculating $\theta_i's$ using (4.8), the correction parameters ($i.e. A1, R, m_1, m_2$ and ϕ) can be obtained using (4.4) as shown in (4.9):

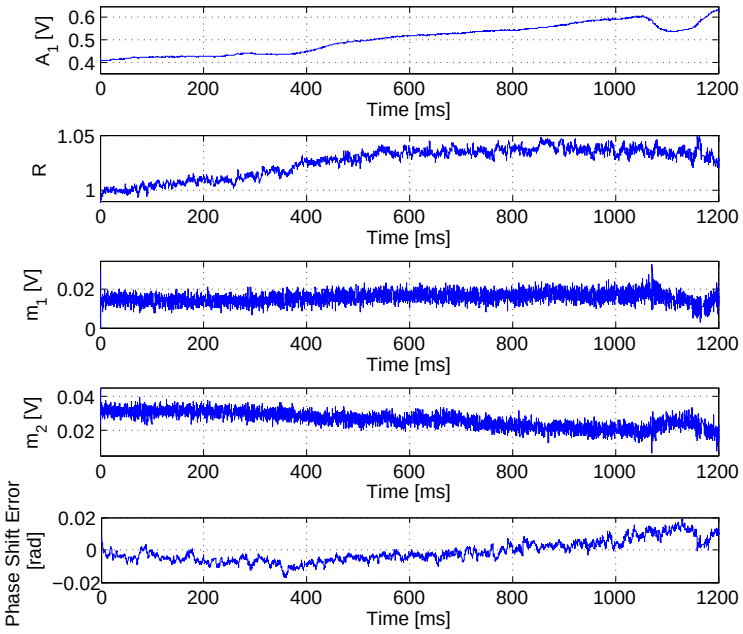

Figure 4.2: Encoder Signal Parameters Recorded Through $120mm$ Motion of the Single Axis Slider

$$\begin{aligned}
\phi &= \arcsin(\theta_3/\sqrt{4\theta_1\theta_2}) \\
R &= \sqrt{\theta_2/\theta_1} \\
m_1 &= (2\theta_2\theta_4 - \theta_5\theta_3)/(\theta_3^2 - 4\theta_1\theta_2) \\
m_2 &= (2\theta_1\theta_5 - \theta_4\theta_3)/(\theta_3^2 - 4\theta_1\theta_2) \\
A_1 &= \sqrt{\frac{4\theta_2(1 + \theta_1 m_1^2 + \theta_2 m_2^2 + \theta_3 m_1 m_2)}{4\theta_1\theta_2 - \theta_3^2}}
\end{aligned} \tag{4.9}$$

As a result, the corrected quadrature signals, $\hat{u}_1$ and $\hat{u}_2$ can be calculated using the correction parameters obtained in (4.9) as follows:

$$\begin{aligned}
\hat{u}_1 &= \frac{1}{A_1}(u_1 - m_1) \\
\hat{u}_2 &= \frac{1}{A_1 \cos\phi}((u_1 - m_1)\sin\phi + R(u_2 - m_2))
\end{aligned} \tag{4.10}$$

Using this method, correction parameters are adjusted with each iteration recursively considering the effects of parameter values from the previous iterations.

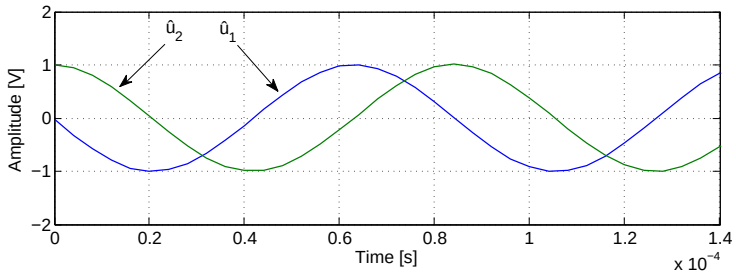

(a)

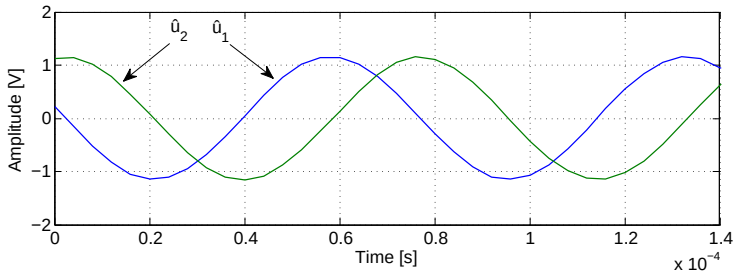

(b)

Figure 4.3: Corrected Encoder Signals Using RLS (a) with and (b) without Resetting

Hence, slow changes in the parameters can be covered efficiently. In Figure 4.2, changes in the signal amplitude, gain ratio, mean offsets, and phase shift errors recorded through $120mm$ motion of our single axis slider are shown. For short range movements (less than couple of hundreds of micrometers), parameters can be assumed to change smoothly and continuously. However, as it is also observed in Figure 4.2, these parameters may change more dramatically for long range motions. For such cases, a standard RLS with exponential forgetting cannot estimate the parameters effectively. Hence, in long range motions, resetting is used to cover the significant parameter changes. For this purpose, the matrix $\boldsymbol{P}$ in the RLS algorithm given in (4.8) is reset periodically to its initial value of $\kappa\boldsymbol{I}$. As a result of resetting, parameter estimate is updated with a larger step size so that significant changes in the parameters can be estimated well since the gain $\boldsymbol{K}(t)$ in (4.8) gets larger [40]. In Figure 4.3, corrected encoder signal data obtained through the end of $120mm$ motion of the slider is given for RLS with resetting and without resetting cases. It is obvious that a better correction of the encoder signals is accomplished using RLS with resetting where long range motion is the

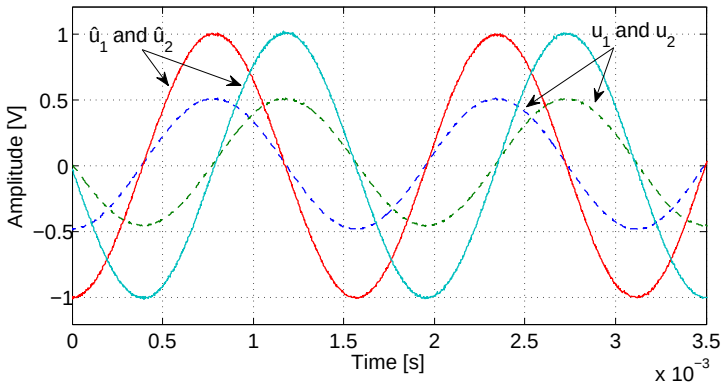

Figure 4.4: Corrected and Original Encoder Signals

focus of interest. As shown in Figure 4.3b, when there is no resetting of matrix $\boldsymbol{P}$ in the RLS algorithm, corrected signals still contain amplitude, mean offset and phase shift errors at the end of long range motions. The amplitude error for no resetting case is measured around $14\% - 16\%$. Mean offset errors can reach up to $0.1V$ and phase shift error is about $2.5 - 3$ *degrees*. Although the phase shift error seems small, when high-resolution measurements are concerned, it is not acceptable. Moreover, these errors will be amplified when an interpolation method is applied to obtain high-resolution. Illustration of the encoder signals obtained before and after correction using RLS with exponential forgetting and resetting is given in Figure 4.4. In order to illustrate the quadrature phase shift of the corrected signals more clearly, variation of amplitude of corrected signals between 0 and $\pi/2$ radians are given in Figure 4.5. As it can be observed in this figure, corrected signals have a phase difference of $\pi/2$ as desired.

4.3 Look-up Table Based Signal Interpolation (Step 2)

In order to derive intermediate position values, corrected encoder signals are interpolated. For this purpose, high-order sinuoids are generated by mapping the corrected sinusoidal encoder signals to high-order ones. Here, calculation of higher order sinusoids using general formulations in (4.11) can be a tedious

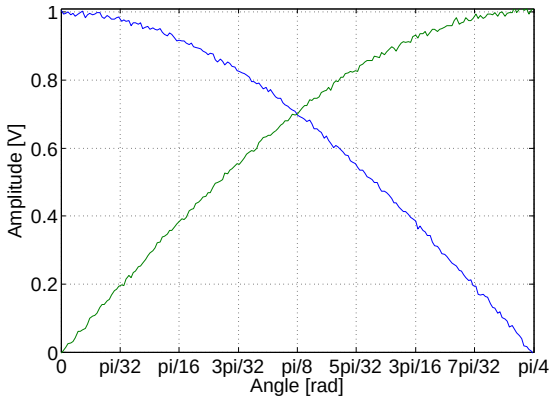

Figure 4.5: Verification of Quadrature Phase Difference Between Corrected Signals

operation.

$$\begin{aligned} \sin(n\alpha) &= \sum_{k=0}^{n} \cos^k(\alpha) \sin^{n-k}(\alpha) \sin(\frac{1}{2}(n-k)\pi) \\ \cos(n\alpha) &= \sum_{k=0}^{n} \cos^k(\alpha) \sin^{n-k}(\alpha) \cos(\frac{1}{2}(n-k)\pi) \end{aligned} \tag{4.11}$$

where the first parenthesized term is a binomial coefficient and n is the order. Calculating values of high-order sinusoids using original first order sinusoids may reduce accuracy. Moreover, real time performance of the interpolation process can be low due to high computational burden. In our method presented here, we use a look-up table based interpolation method for mapping of original encoder signals to high-order sinusoids at high process speeds. For this purpose, a quick access look-up table is populated offline. The look-up table used in this section directly uses the actual numerical values of high-order sinusoids since the corrected signals coming from the adaptive signal correction step are sufficiently close to the real sinusoidal signal values. Moreover, as previously mentioned, signal characteristics change significantly in long ranges and different encoders may have different signal characteristics. Hence, it is much more practical to use the mathematical values of high-order sinusoids. Also, the look-up table generation task in this method is practical and the same look-up table is applicable to different encoders or operation conditions.

Table 4.1: A Generic Look-up Table

Index	$\mathbf{cos(n\alpha)}$	$\mathbf{sin(n\alpha)}$
0	1	0
1	$\cos(\frac{n\pi}{8N})$	$\sin(\frac{n\pi}{8N})$
2	$\cos(\frac{n\pi}{4N})$	$\sin(\frac{n\pi}{4N})$
:	:	:
i	$\cos(\frac{ni\pi}{8N})$	$\sin(\frac{ni\pi}{8N})$
:	:	:
$8N$	1	0

In the interpolation step, index calculator shown in Figure 4.1 uses the values of corrected signals, $\hat{u}_1$ and $\hat{u}_2$, as inputs and generates an index number, i. Using the index number as an addressing data, values of n^{th} order sinusoids, u_{1n} and u_{2n}, corresponding to $\hat{u}_1$ and $\hat{u}_2$ are obtained from the quick access look-up table.

For our research, we construct our look-up table by dividing each octants (i.e. interval of $\pi/4$ *radians*) of a set of n^{th} order sinusoidal signals, $\cos(n\alpha)$ and $\sin(n\alpha)$, into N samples leading $8N$ samples over one period of a high-order sinusoids. Then, values of these samples are stored in the look-up table prior to the process. A generic look-up table for an n^{th} order interpolation is given in Table 4.1. In this table, i denotes the index number generated by index calculator for $\hat{u}_1$ and $\hat{u}_2$.

After the look-up table is constructed, index number should be calculated for mapping of corrected signals to the n^{th} order sinusoids. As also observed in [16], when the index calculation is based on just one signal, $\hat{u}_1$ or $\hat{u}_2$, poor resolution will be obtained around $\hat{u}_1 \approx 1$ or $\hat{u}_2 \approx 1$ due to the highly nonlinear relationship between amplitude and angle α of sinusoidal signals. Although it is sufficient to use high N values to solve this problem, it will also increase the size of look-up

table. Hence, index number may be calculated using the one of the signals, $\hat{u}_1$ or $\hat{u}_2$, which is outside of that poor resolution region. Poor resolution regions can be explained mathematically as

$$\begin{aligned} |\hat{u}_1| &> \sin(\frac{\pi}{4}) \\ |\hat{u}_2| &> \sin(\frac{\pi}{4}) \end{aligned} \tag{4.12}$$

Defining the poor resolution region as in 4.12, index can be calculated by using almost linear relationship between amplitude and angle α outside of these regions in combination with the signs and magnitudes of the signals $\hat{u}_1$ and $\hat{u}_2$. Signs and magnitudes of the signals are only used to find the correct octant of the current angle. For example, for $0 < \alpha \leq \pi/4$, $sign(\hat{u}_1) > 0$ and $\hat{u}_2 \geq \sin(\pi/4)$. Since $\hat{u}_2$ is in the poor resolution area mentioned above, it is suitable to use the value of $\hat{u}_1$ to calculate the index value. Using the linear relationship between amplitude of signal $\hat{u}_1$ and the angle, it can be calculated as

$$i = \frac{\hat{u}_1 N}{\sin(\pi/4)} \tag{4.13}$$

Similarly, for $\pi/4 < \alpha \leq \pi/2$, $sign(\hat{u}_2) \geq 0$ and $\hat{u}_1 > \sin(\pi/4)$. Hence, since $\hat{u}_2$ is at outside of the poor resolution region, it can be used in the calculation leading the index value of

$$i = 2N - \frac{\hat{u}_2 N}{\sin(\pi/4)} \tag{4.14}$$

However, using (4.13), (4.14) and similar ones given in Table 4.2 for the other octants of sinusoids, index numbers obtained may not be integers. Therefore, calculated index values should be rounded to the closest integer values while calculating the index value in order to read the correct value in the look-up table.

In Table 4.2, there are two conditions to define the index calculation. These are called as sign and magnitude conditions. Once a row which concurs with the sign and magnitude conditions is identified, the corresponding formula is used

Table 4.2: Index Calculation Table

Sign	**Magnitude**	**Index, i**	**Angle, α**
$sign(\hat{u}_1) > 0$	$\hat{u}_2 \geq \sin(\frac{\pi}{4})$	$\frac{\hat{u}_1 N}{\sin(\pi/4)}$	$0 < \alpha \leq \frac{\pi}{4}$
$sign(\hat{u}_2) \geq 0$	$\hat{u}_1 > \sin(\frac{\pi}{4})$	$2N - \frac{\hat{u}_2 N}{\sin(\pi/4)}$	$\frac{\pi}{4} < \alpha \leq \frac{\pi}{2}$
$sign(\hat{u}_2) < 0$	$\hat{u}_1 \geq \sin(\frac{\pi}{4})$	$2N - \frac{\hat{u}_2 N}{\sin(\pi/4)}$	$\frac{\pi}{2} < \alpha \leq \frac{3\pi}{4}$
$sign(\hat{u}_1) \geq 0$	$\hat{u}_2 < -\sin(\frac{\pi}{4})$	$4N - \frac{\hat{u}_1 N}{\sin(\pi/4)}$	$\frac{3\pi}{4} < \alpha \leq \pi$
$sign(\hat{u}_1) < 0$	$\hat{u}_2 \leq -\sin(\frac{\pi}{4})$	$4N - \frac{\hat{u}_1 N}{\sin(\pi/4)}$	$\pi < \alpha \leq \frac{5\pi}{4}$
$sign(\hat{u}_2) \leq 0$	$\hat{u}_1 < -\sin(\frac{\pi}{4})$	$6N + \frac{\hat{u}_2 N}{\sin(\pi/4)}$	$\frac{5\pi}{4} < \alpha \leq \frac{3\pi}{2}$
$sign(\hat{u}_2) > 0$	$\hat{u}_1 \leq -\sin(\frac{\pi}{4})$	$6N + \frac{\hat{u}_2 N}{\sin(\pi/4)}$	$\frac{3\pi}{2} < \alpha \leq \frac{7\pi}{4}$
$sign(\hat{u}_1) \leq 0$	$\hat{u}_2 > \sin(\frac{\pi}{4})$	$8N + \frac{\hat{u}_1 N}{\sin(\pi/4)}$	$\frac{7\pi}{4} < \alpha \leq 2\pi$

to calculate the index value as described above. Since the table is constructed by considering only the signs and magnitudes of the available encoder signals, it is easier to understand and implement in real time applications compared to the ones mentioned in the literature. It also serves as a quick access tool for the look-up table. Moreover, round off error is minimized by eliminating extra index numbers proposed in [16].

Using Table 4.2 for calculation of index and obtaining the corresponding values from the look-up table, n^{th} order sinusoidal signals can be obtained. An example interpolation results for $n = 25$ is given in Figure 4.6. For the interpolation, N is chosen to be 1000. Considering the results shown in Figure 4.6, it is clearly seen that high-order sinusoids can be obtained effectively using the presented correction and interpolation methods. The calculated index number, i, corresponding to the corrected signals, $\hat{u}_1$ and $\hat{u}_2$, is given in Figure 4.7. In

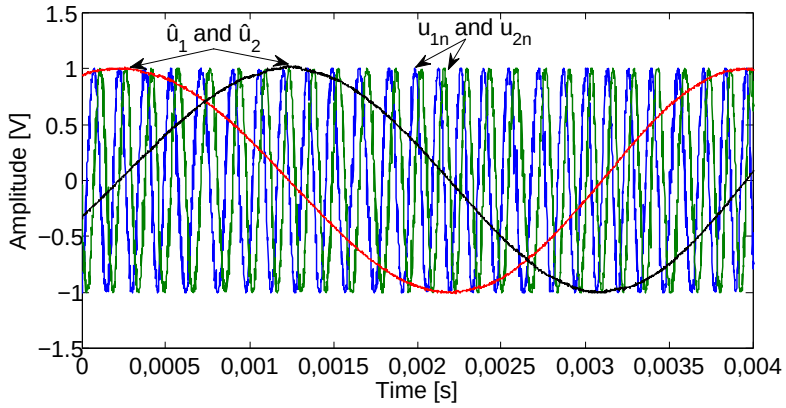

Figure 4.6: Interpolation Results for $n = 25$

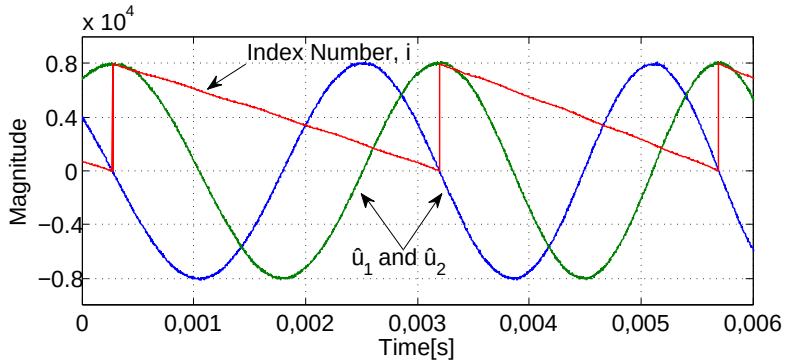

Figure 4.7: Variation of Index Number for $n = 25$

this figure, amplitudes of sinusoidal signals are set to 8000 deliberately to show the relationship between signal amplitudes and index clearly. Expectedly, index number varies from 0 to 8000 ($8N$) linearly in one period of signals. Linear relationship shown in this figure also illustrates the effectiveness of the proposed interpolation method. More detailed experiments and results for the proposed interpolation method are given in the experiments section.

4.4 Binary Pulse Generation and Position Information

In order to use the interpolated encoder signals, u_{1n} and u_{2n}, as position information in a system, quadrature signals should be converted to the binary pulses. Then, the position information can be derived by counting the zero-crossings of these binary pulses. Although it is possible to use extra hardware for this purpose, it can be accomplished in software by generating A and B binary pulses (as illustrated in Figure 4.1) using the following equations.

$$\begin{aligned} A &= \begin{cases} 1 & \text{if } u_{1n} \geq \varepsilon \\ -1 & \text{if } u_{1n} \leq -\varepsilon \end{cases} \\ B &= \begin{cases} 1 & \text{if } u_{2n} \geq \varepsilon \\ -1 & \text{if } u_{2n} \leq -\varepsilon \end{cases} \end{aligned} \tag{4.15}$$

In (4.15), ε is a small threshold value. This value should be chosen considering the noise level of the interpolated signals coming from the interpolation stage. With the proper selection of this number, undesired zero crossings can be eliminated although encoder signals contain significant amount of error.

In Figure 4.8, binary pulses generated using (4.15) are shown. In this figure, corrected ($\hat{u}_1$ *and* $\hat{u}_2$) analog signals are also given. Interpolation is conducted for $n = 25$ and threshold value, ε, of $0.05V$ is used. In order to prevent confusion, amplitudes of binary pulses are set to 0.4 and 0.6 for A and B, respectively.

After the binary pulses are generated, the sign changes or zero crossings in these pulses are counted. Then, multiplying this number with the intended distance between two zero crossings, the position information can be calculated. In (4.16), mathematical relationship between the number of zero-crossings and the position information, x, is given.

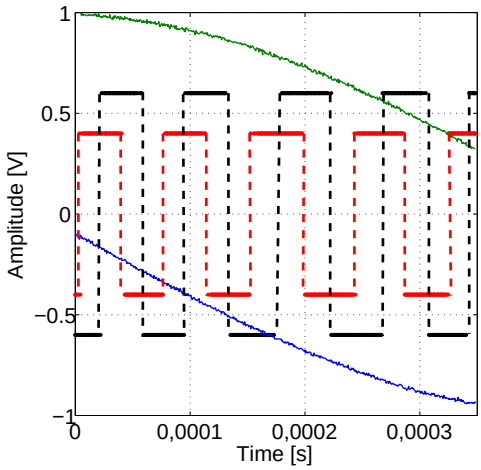

Figure 4.8: Binary Pulses Obtained for $n = 25$

$$x = \frac{n_{zc} l_p}{4n} \tag{4.16}$$

where n_{zc} is the number of zero crossings, l_p is the pitch of scale grating and n is the number of interpolation. For example, the presented interpolation technique is applied on a linear optical encoder with scale grating of $l_p = 4\mu m$ in pitch and the number of interpolation is chosen to be $n = 5$. For without interpolation case, 4 zero-crossings of signals mean $4\mu m$ of displacement since between two scale grating one period of each signal passes. However, when the interpolation method is applied, detection of 4 zero-crossings imply $4/5\mu m$ of displacement. In Figure 4.9, an illustration of this example showing the encoder signals without interpolation (first order signals) and signals with interpolation (for $n = 5$) is given. In this figure, the binary pulses created using encoder signals are also shown. However, their magnitudes are deliberately set to $0.6V$ and $0.8V$ to prevent any confusion in the signals. In this example, when 1000 number of zero crossings in positive direction are detected in the binary pulses for interpolation case, $1000x4/(4x5) = 200\mu m$ of displacement is accomplished. Using the same procedure for both directions, the position information can be derived from the binary pulses by counting zero-crossings.

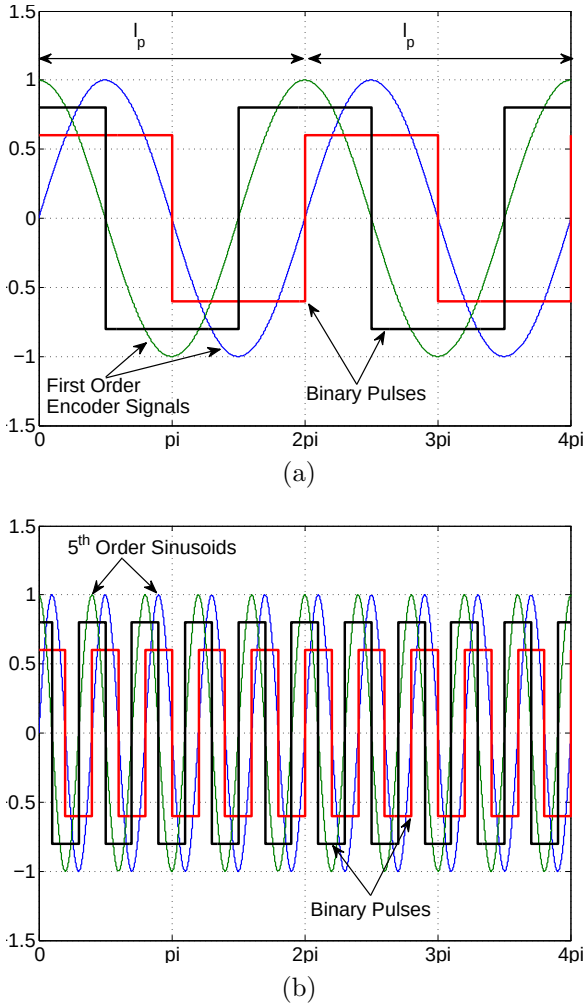

Figure 4.9: Example Showing Encoder Signals and Binary Pulses for (a) Without Interpolation (b) With Interpolation Cases

4.5 Practical Limitations

Application of the proposed method to generate high-resolution quadrature encoder signals is limited due to some practical constraints such as number of samples recorded, velocity of movement to be measured and signal noise.

Linear optical encoders generate sinusoidal signals with a period equal to the grating pitch of the encoder scale, l_p. With the implementation of proposed method for n number of interpolations, high-order sinusoids (n^{th} order) with a period equal to l_p/n are generated. Hence, when N_1 samples are recorded in one

period of original first order sinusoidal encoder signal, interpolation number can be expressed as

$$n = \frac{N_1}{N_n} \tag{4.17}$$

where N_n is defined as the number of samples in one period of n^{th} order sinusoid. Following the same idea, maximum interpolation number, n_{max}, can be defined as

$$n_{max} = \frac{N_1^{max}}{N_n^{min}} \tag{4.18}$$

where N_1^{max} is the maximum number of samples to be recorded in one period of original encoder signals and N_n^{min} is the minimum number of samples to present in n^{th} order sinusoid. Considering the expression in (4.18), interpolation number is limited by available sampling performance.

Another constraint for the number of interpolation is velocity of the movement to be measured. Defining the loop time, t_{loop}, as the time required to process one sample of encoder signal, relation between the maximum interpolation number and maximum velocity of the motion, v_{max}, can be expressed as in (4.19). In this equation, limit on the number of interpolation due to maximum velocity of the system through a motion is considered.

$$n_{max} = \frac{l_p}{v_{max} N_n t_{loop}} \tag{4.19}$$

Noise in encoder signals is also an important factor limiting the number of interpolation. In order to obtain high-resolution via proposed interpolation method, noise in the encoder signals should be minimized by shielding, grounding and filtering. After these processes, effect of remaining small level noise on resulting position value can be eliminated with the proper selection of the threshold value for binary pulse generation in (4.15) as mentioned previously.

Chapter 5

Real-Time Implementation

Although the encoder resolution improvement technique presented in this thesis is expressed mathematically, real time implementation of it requires a special effort due to some practical constraints in the programming software and other equipment. For the real time implementation of the presented encoder resolution improvement method, Labview software is used. Moreover, control algorithms developed for multi-axis precision positioning systems presented in [39] are also implemented.

In this chapter, details of the real-time implementation of encoder resolution improvement method are given. For this purpose, first, Labview implementation of the method is discussed including the encoder signals correction, look-up table based interpolation, binary pulse generation and position information derivation parts. Next, Labview implementation of the control algorithm used to control the single, two and three axis slider systems is also shown while explaining the overall control system.

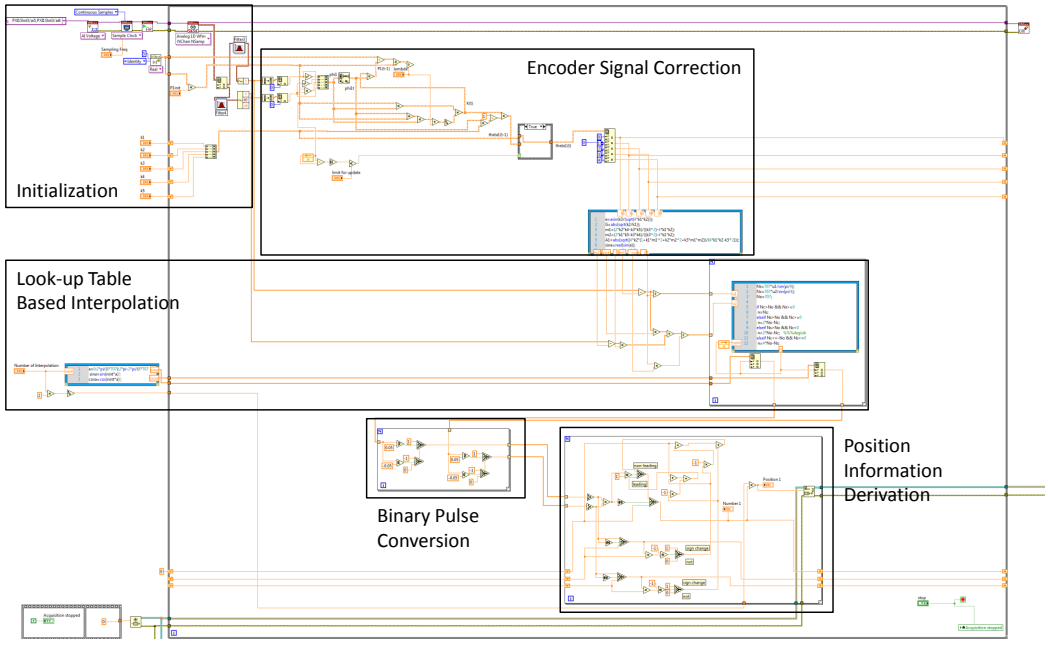

Figure 5.1: Encoder Resolution Improvement Method Labview Implementation

5.1 Real-Time Implementation of Encoder Resolution Improvement Method

In this section, real-time implementation of the encoder resolution improvement technique presented in Chapter 4 is discussed in detail. For the implementation process, Labview software is used and the same algorithm is employed for all systems including single, two and three axis positioning systems.

In Figure 5.1, encoder resolution improvement loop is given for single axis positioning system. In this figure, encoder signal correction, look-up table based interpolation, binary pulse generation and position information derivation parts are labeled to illustrate the data flow clearly. As it can be observed in this figure, after the initialization for the loop is done, acquired analog encoder signals are corrected in the correction part. Then, the corrected signals are sent to the look-up table based interpolation section. After the interpolation, high order sinusoids are converted to binary pulses so that the position information can be derived

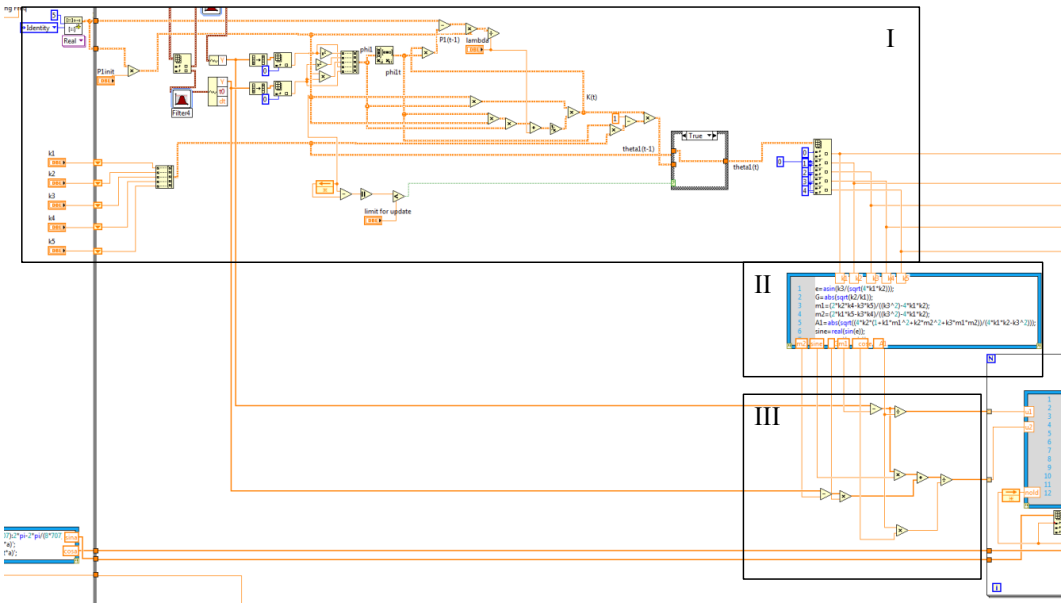

Figure 5.2: Encoder Signal Correction Labview Implementation

by counting the zero crossings. All of these processes are inserted in a while loop so that the procedure continues until the user stops it using the front panel (Appendix A).

For the initialization part, there are two tasks to accomplish before the signal correction process starts. These are data acquisition and data filtering. Using daqmx.vi's in Labview, encoder signal voltage data is acquired from two channels as continuous samples. Here, acquisition rate is adjusted to $300000Hz$ for our system and data is obtained as waveform. Advantage of acquiring data as waveform is that samples are stored as packages so that the same number of sample can be delivered in shorter time leading smaller loop time. Moreover, time information is also supplied in the waveform. After the data acquisition accomplished, electrical noise in the encoder signal is filtered using filter.vi's. By filtering the encoder signals effect of noise in the interpolation stage is reduced. For our system, Butterworth low pass filter is used for both encoder signals.

In Figure 5.2, a detail view of encoder signal correction part of Labview VI documentation is given. Part I of this figure shows the real time implementation of mathematical expression for RLS with exponential forgetting and resetting given

in (4.8). In this part, first, initial conditions for $\boldsymbol{\theta}$ and $\boldsymbol{P}$ are defined for RLS process. In the real time implementation, k_i's represent θ_i's ($i = 1, 2, .., 5$). For the encoders used in our positioning systems, initial condition for $\boldsymbol{\theta}$ and $\boldsymbol{P}$ are chosen as $[3.40, 3.40, 0, -0.1, -0.1]$ and $100\boldsymbol{I}$, respectively. These initial conditions are determined roughly by experiments. Since the correction algorithm is adaptive, there is no need to fine tune the initial conditions. After the initial conditions are defined signals are processed to calculate parameter update vector, $\boldsymbol{\theta}$, as in (4.8). In the implementation of recursive parameter adjustment law, exponential forgetting factor, λ, is chosen as 1 in order to have maximum contribution of old data to parameter adjustment. In order to satisfy resetting property, $\boldsymbol{P}$ is defined inside of the while loop so that it is reset to its initial value of $100\boldsymbol{I}$ at the beginning of each iteration. In Part I, parameter update is limited by a switch in order to reduce the computation burden. For this purpose, difference between the signal values of the current and previous iteration is calculated. When magnitude of this difference is lower than a specific value, $\boldsymbol{\theta}$ is not updated. This limit is an empirical value and it is determined as $0.001V$ for our system. After the parameter update vector is defined, correction parameters are calculated using θ_i's in a mathscript in Part II. Here, Part II is the real time implementation of (4.9). Since this process requires complex mathematics, it is accomplished in a mathscript. Using the correction parameters calculated in Part II, distorted encoder signals are corrected in Part III. In this part, (4.10) is implemented to the Labview environment.

After the encoder signals are corrected, the corrected signals are fed into the look-up table based interpolation section as shown in Figure 5.1. In Figure 5.3, zoomed view of look-up table based interpolation section of Labview document is given. In this figure, Part IV is the offline look-up table generation part and it is the real time implementation of Table 4.1. In this part, using a mathscript, a look-up table including mathematical values of high-order sinusoids is formed. Order of the sinusoids depend on the desired interpolation number. While calculating the high-order sinusoids, each octant of them are divided into N samples leading $8N$ samples over one period of the high-order signals. For our experiments, $N = 1000$ is used. When the value of N is increased, the size of look-up table

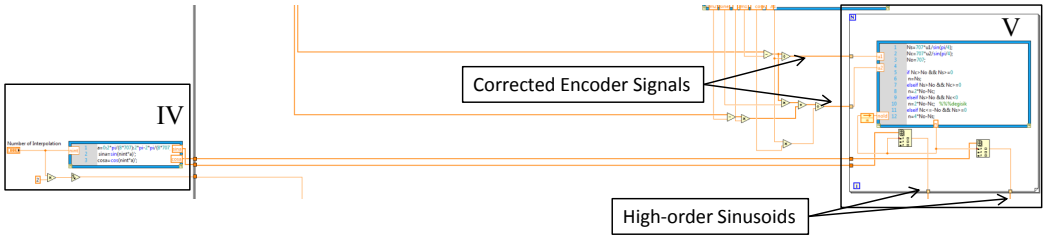

Figure 5.3: Look-up Table Based Interpolation Labview Implementation

also increases. Hence, there is a trade-off between the sample number and the computation effort. After the look-up table for high-order sinusoids are generated offline, corrected signals are mapped to high-order sinusoids by calculating index numbers for the look-up table. In Figure 5.3, Part V shows the index number calculation process. This part is the implementation of Table 4.2 to the Labview environment. Here, a for loop is used to calculate an index number for each sample in the waveform data package. Using the signs and magnitudes of the corrected signals, index numbers are calculated for each sample in a mathscript. Then, using the index number, corresponding look-up table value is obtained as the high-order sinusoids by using array.vi's.

When the interpolation process is completed, calculated high-order sinusoids are sent to the binary pulse generation loop so that the position information can be derived. In Figure 5.4, Labview implementation of binary pulse conversion and position information derivation processes are shown as Part VI and Part VII, respectively. For binary pulse conversion, (4.15) is implemented. However, in order to prevent any data loss, signals with amplitudes between $-\varepsilon$ and ε is converted to 0. In our system, ε is chosen to be $0.05V$ for all encoders. Similar to index generation loop, binary pulse conversion and position information derivation processes are accomplished inside of for loops in order to process each sample in a waveform. After the binary pulses are generated in Part VI, zero crossings are counted to obtain position information in Part VII. However, direction of the motion should be determined for correct position information. For this purpose, in Part VII, leading signal is determined by comparing the signs of the signals. If $\sin(n\alpha)$ is the leading signal, number of zero crossings are added to the total

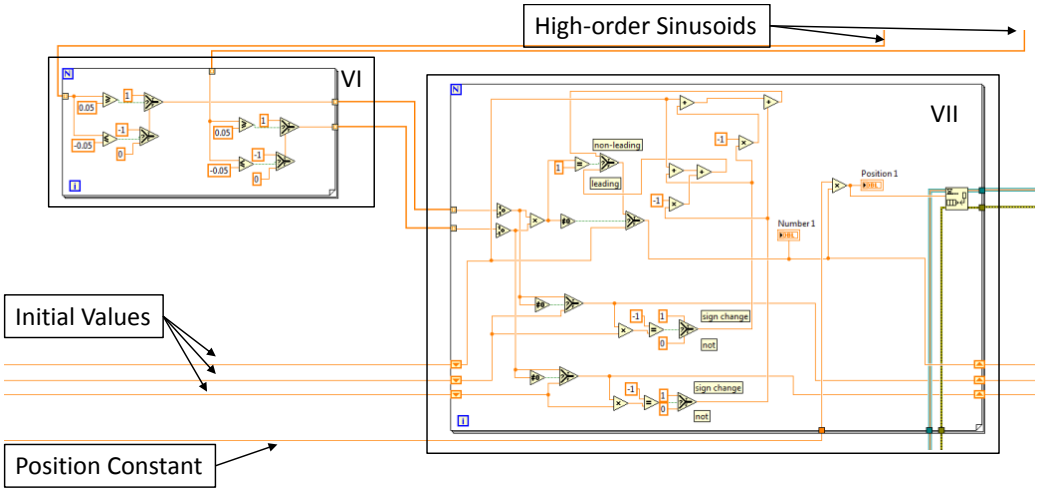

Figure 5.4: Binary Pulse Generation and Position Information Derivation Labview Implementation

value, otherwise, it is subtracted. Then, multiplying the counter value by a position constant, position information is obtained. Here, position constant is the displacement value corresponding to the distance between two zero crossings and it is directly related to the interpolation number. Mathematical expression of the relation between the position and the number of zero crossings implemented in Part VII is given in (4.16).

Real time implementations of the encoder resolution improvement method for two and three axis systems are similar. They are also given in Appendix A with the overall control diagrams.

5.2 Real-Time Implementation of Overall Control System

In this section, Labview implementation of overall control system including the encoder resolution improvement loop and the control loop is summarized. As an example, overall control system implementation of single axis slider is given in Figure 5.5. In this figure, iterative learning controller (ILC) is implemented as

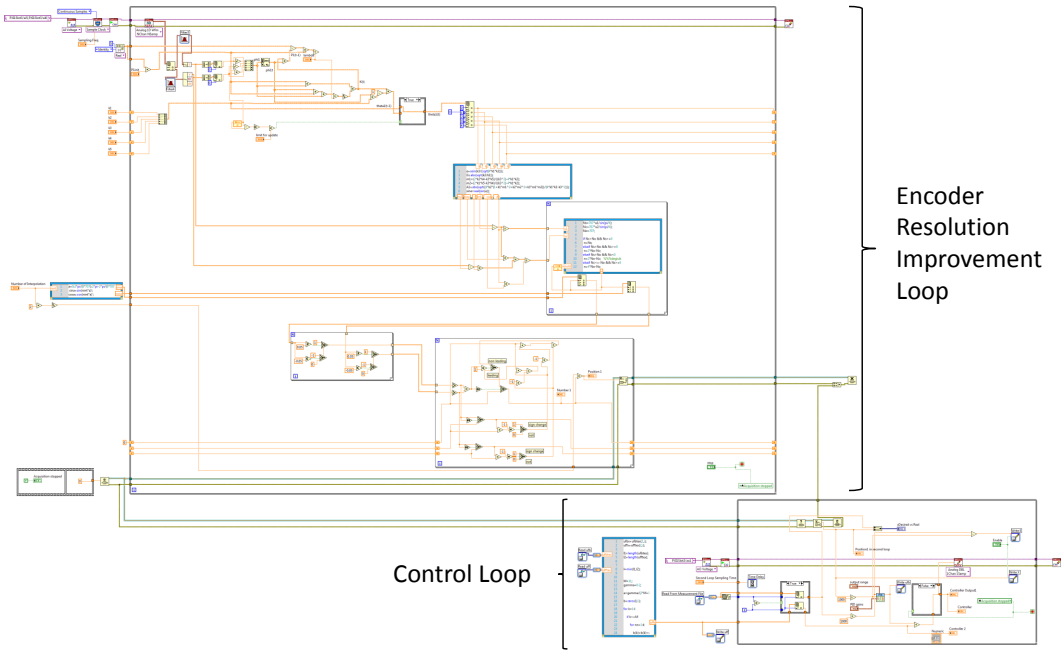

Figure 5.5: Labview Implementation of Overall Control System for Single Axis Slider System

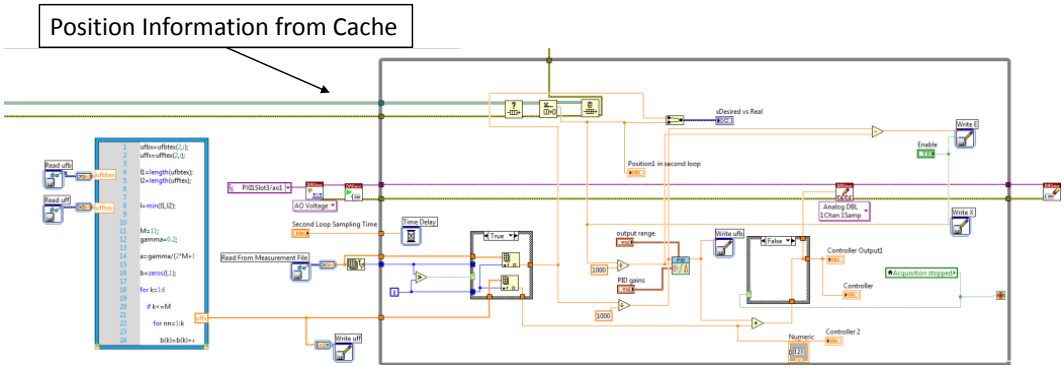

Figure 5.6: Labview Implementation of Control Loop for Single Axis Slider System

controller. Details of the controller can be found in [39]. In the figure, encoder resolution improvement loop and the control loop is labeled. Since these two loops are processed at different speeds, position information is supplied to the control loop only when it is desired. For this purpose, a cache is used to store the position values coming from the encoder resolution improvement loop.

In Figure 5.6, detailed view of the control loop is given. In this loop, daqmx.vi's are used to send control output to the system. Iterative learning controller is implemented by using a mathscript. In this script, control signal data from previous iterations are used to calculate the new feedforward control signals. Previous iteration data is stored in lvm files and read back when necessary.

In Appendix A, Labview front panels used to control single, two and three axis positioning systems are supplied with Labview VI documentations of overall control systems for two and three axis systems.

Chapter 6

Validation and Experiments

In this thesis, an encoder resolution improvement technique is presented to increase the available resolution of the encoder used in the positioning system. In order to show the performance and effectiveness of this technique, experiments with different interpolation numbers should be conducted. In Chapter 4, some experiment results are supplied to illustrate the working principle of the method including the adaptive signal correction and signal interpolation parts. In addition to experiments showing the performance of encoder resolution improvement technique itself, experiments showing the effects of encoder resolution improvement on positioning performance of our slider systems are important. Moreover, an external validation is also required to express the performance of the encoder resolution improvement method numerically.

In this chapter, first, validation of proposed encoder resolution improvement method is explained. Experimental setup used for the validation tests are described in detail. Validation test results obtained for several cases with different interpolation numbers are provided. Next, results of several experiments conducted on single axis slider are shown to illustrate the effectiveness of the presented adaptive signal correction and interpolation methods. Moreover, effects of encoder resolution improvement on positioning performance of presented single, two and three axis positioning systems are tested.

6.1 Validation of Encoder Resolution Improvement Method

In order to prove that the presented encoder resolution improvement method is working properly, an external validation is required. For this purpose, an external displacement sensor with known resolution can be used. However, resolution of this sensor should be higher than the intended measurement resolution of the encoder that the signal interpolation method is applied.

In this section, validation study for presented encoder resolution improvement approach is summarized. Testbed for validation experiments is explained with its components. Experimental results for several cases with different resolution values including the best resolution we have obtained are supplied. Experiments are conducted for all axes in order to show that the same method can be applied on different encoders without any modification.

6.1.1 Experimental Setup

In order to validate the presented encoder resolution improvement method, a two-arm differential laser vibrometer with adjustable resolution is used as an external measurement device. In the validation experiments, the aim is to compare the displacement values obtained using the linear encoder and the vibrometer. Calculating the RMS error levels by taking the vibrometer readings as reference, a numerical expression for performance of the encoder resolution improvement method is obtained. In order to show the performance clearly, validation experiments are conducted for several cases with different interpolation numbers leading different resolution values.

In Figure 6.1, the test setup prepared for validation experiments on x-axis is shown. Here, a Polytech OFV-552 two-arm laser vibrometer is used with OFV-5000 vibrometer controller as an external measurement device. OFV-5000 vibrometer controller can be tailored with various decoders to reach the desired

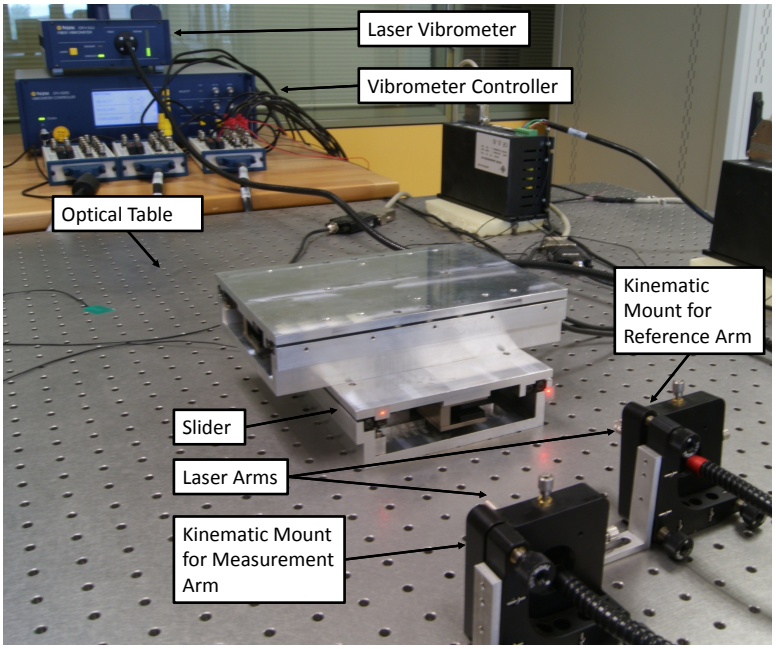

Figure 6.1: Testbed for Validation Experiments

performance [28]. In our system, DD-900 broadband digital displacement decoder and VD-09 broadband digital velocity decoders are used. With this combination, it is possible to adjust measurement resolution between $15pm$ and $1500\mu m$ by adjusting the measurement range. As the resolution is increased, the measurement range decreases. For example, it is possible to reach $15pm$ measurement resolution when measurement range is adjusted to $1\mu m$ whereas when the resolution is chosen as $150nm$, measurement range increases to $10000\mu m$. However, when the resolution is increased, effect of noise on the measurement signals also increases depending on the electrical noise characteristics of the test environment. Considering this fact, for our validation experiments, we used $3nm$ resolution with $200\mu m$ measurement range.

As it can be seen in Figure 6.1, one of the laser arms is directed to the stationary base of the slider as the reference and the other laser arm is positioned to point at the moving slider. Purpose of this arrangement of the laser arms is to reduce the effect of environmental vibrations on our displacement measurements. With this arrangement, the measured vibrometer reading is differential and free from undesired common vibrations. Moreover, the whole system including the

sliders and laser arm mounts is mounted on an optical table to obtain noise-free displacement measurements. As laser arm mounts, Thorlabs six degree-of-freedom (DOF) kinematic mounts are used to obtain required orientation and position of the lasers.

For the laser vibrometer to measure the displacement with minimum error and maximum accuracy, lasers should be positioned so that bar shaped signal strength indicator on OFV-552 is full. Full strength indicator means that the laser beam is perpendicular to the surface to be measured. Hence, laser beams are positioned using 6-DOF kinematic mounts so that full strength is obtained for validation experiments.

6.1.2 Validation Test Results

Although the measurement range of the laser vibrometer is chosen as $200\mu m$ for $3nm$ resolution, displacements with couple of micrometers are given in order to illustrate the validation results clearly. Moreover, validation experiments are conducted on each axis separately to prove that the proposed encoder resolution improvement method can be applied on different encoders without any modification in the algorithm.

In Figure 6.2, Figure 6.3 and Figure 6.4, displacement measurements obtained on x-axis slider with the vibrometer and the linear encoder with increased measurement resolution are given for interpolation numbers of $n = 10$, $n = 50$ and $n = 100$, respectively. Resulting measurement resolutions are $100nm$, $20nm$ and $10nm$ for these interpolation numbers. Similar validation experiment results obtained on y-axis and z-axis sliders are given in Figure 6.5, Figure 6.6, Figure 6.7 and Figure 6.8, Figure 6.9, Figure 6.10, respectively.

For all cases including the best resolution we obtained ($10nm$), interpolation results match with the displacement measurements measured with laser vibrometer. In order to show the effectiveness of the encoder resolution improvement

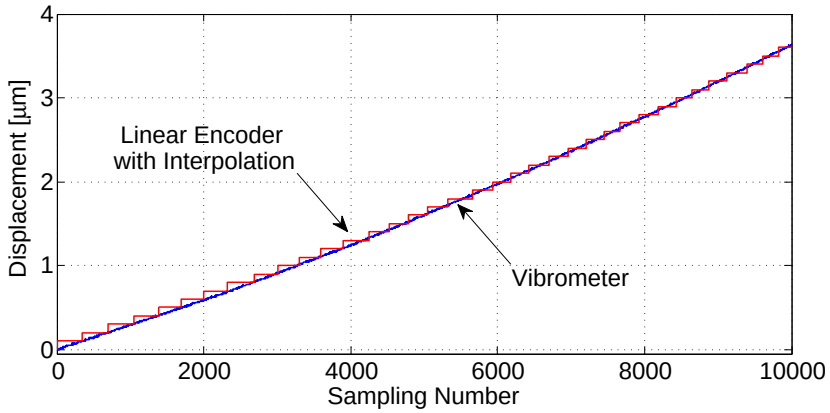

Figure 6.2: Validation Results on x-Axis Slider for Interpolation Number of $n = 10$ Resulting $100nm$ Measurement Resolution

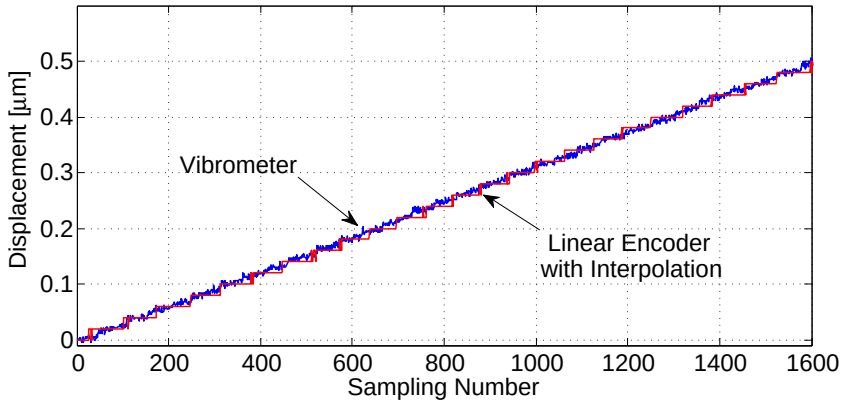

Figure 6.3: Validation Results on x-Axis Slider for Interpolation Number of $n = 50$ Resulting $20nm$ Measurement Resolution

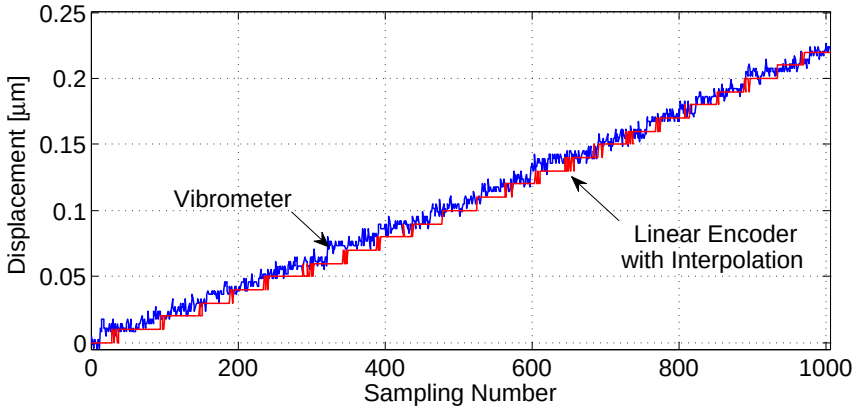

Figure 6.4: Validation Results on x-Axis Slider for Interpolation Number of $n = 100$ Resulting $10nm$ Measurement Resolution

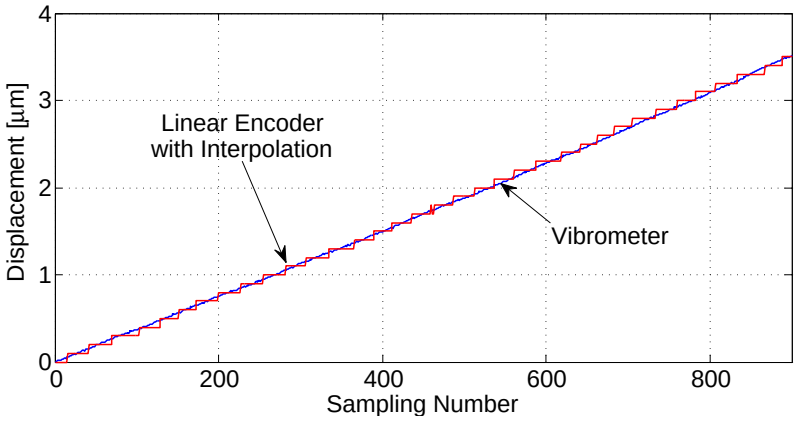

Figure 6.5: Validation Results on y-Axis Slider for Interpolation Number of $n = 10$ Resulting $100nm$ Measurement Resolution

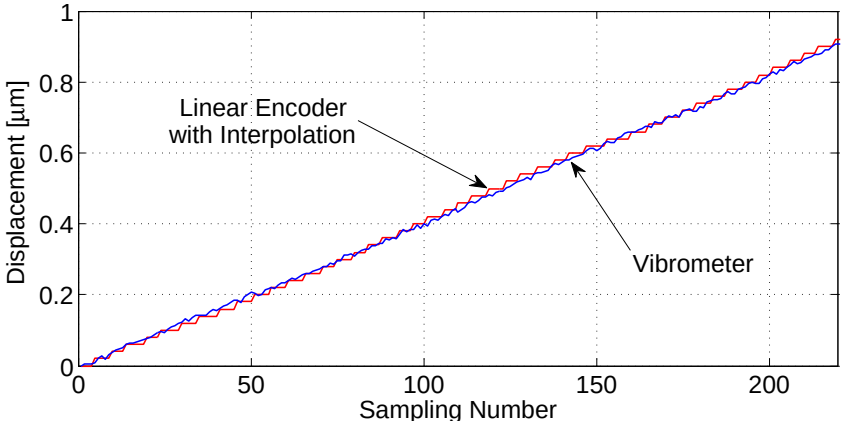

Figure 6.6: Validation Results on y-Axis Slider for Interpolation Number of $n = 50$ Resulting $20nm$ Measurement Resolution

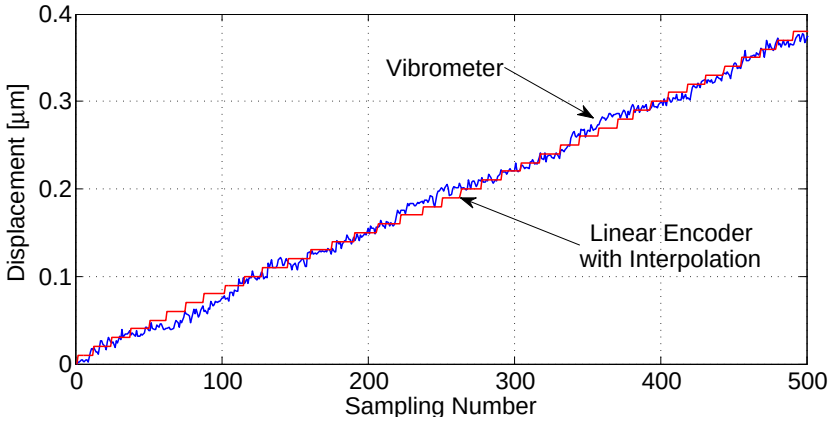

Figure 6.7: Validation Results on y-Axis Slider for Interpolation Number of $n = 100$ Resulting $10nm$ Measurement Resolution

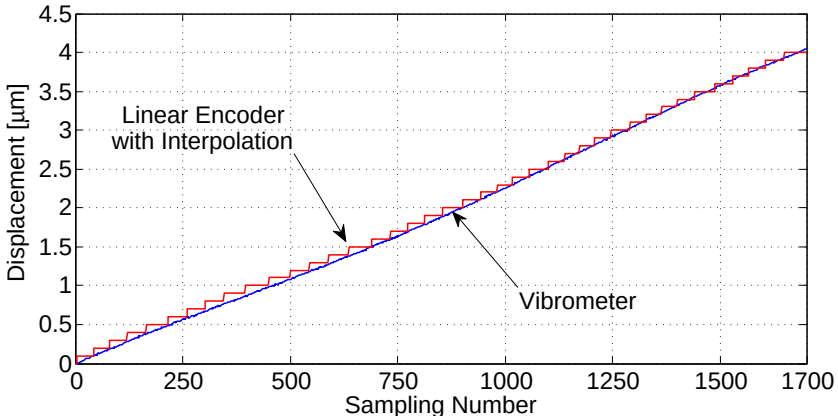

Figure 6.8: Validation Results on z-Axis Slider for Interpolation Number of $n = 10$ Resulting $100nm$ Measurement Resolution

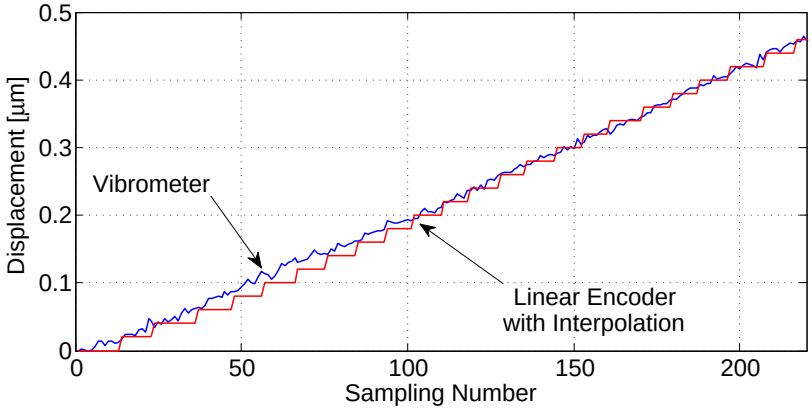

Figure 6.9: Validation Results on z-Axis Slider for Interpolation Number of $n = 50$ Resulting $20nm$ Measurement Resolution

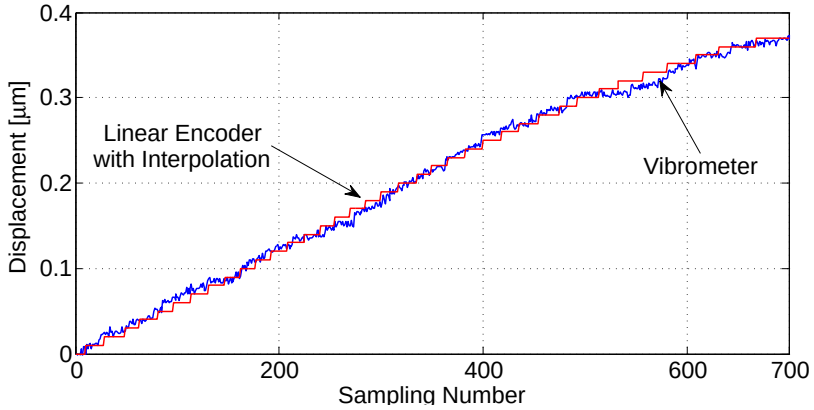

Figure 6.10: Validation Results on z-Axis Slider for Interpolation Number of $n = 100$ Resulting $10nm$ Measurement Resolution

method numerically, root mean square (RMS) of measurement differences between the vibrometer and linear encoder with interpolation are obtained for all of these cases. These values are calculated for x-axis slider as $43.5nm$, $8.3nm$ and $7.2nm$ for $n = 10$, $n = 50$ and $n = 100$, respectively. Similarly, RMS of measurement difference values for y-axis slider are calculated as $36.8nm$, $10.6nm$ and $7.9nm$. For z-axis, the RMS differences are obtained as $62.0nm$, $12.3nm$ and $7.1nm$. Since these error values are below the intended measurement resolutions achieved with the application of presented encoder resolution improvement method on linear optical encoders for each case, it can be concluded that the performance of the method is validated successfully. Moreover, these results show that presented approach can be applied on different encoders without any change in the algorithm.

6.2 Experimental Results

In this section, performance of the encoder interpolation technique explained in this thesis is presented. For this purpose, results of the experiments conducted for different interpolation numbers are given. In these experiments, single axis slider is used. Moreover, effects of encoder resolution improvement method on tracking and contouring performance of single, two and three axis slider systems are also discussed.

In the experiments, signals coming from Heidenhain LIP 481R linear optical encoders are collected using NI PXIe-6358 X series data acquisition card attached on the PXIe-1062Q series chasis. In this chasis NI PXIe-8133 series controller is embedded. Labview programming environment is used to implement the encoder resolution improvement method algorithm. Data acquisition is accomplished for each encoder simultaneously at a rate of $300000 samples/s/channel$. Since one encoder gives two sinusoidal signals, two channels are used for each encoder. Original measurement resolutions of the encoders used in the experiments are $1\mu m$.

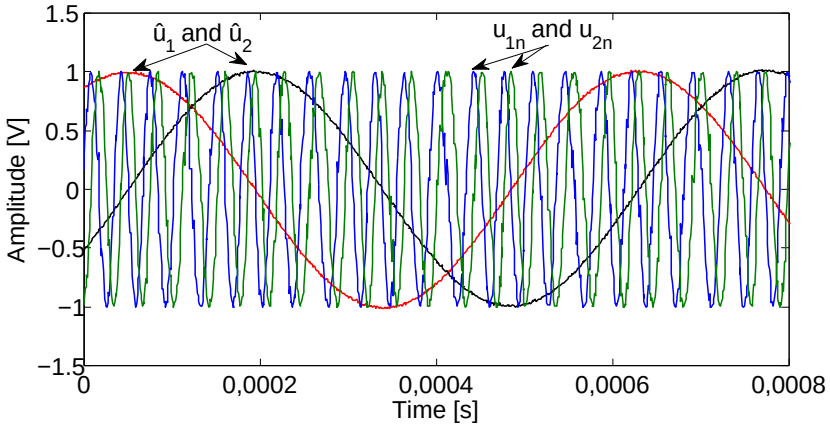

Figure 6.11: Interpolation Results for $n = 16$

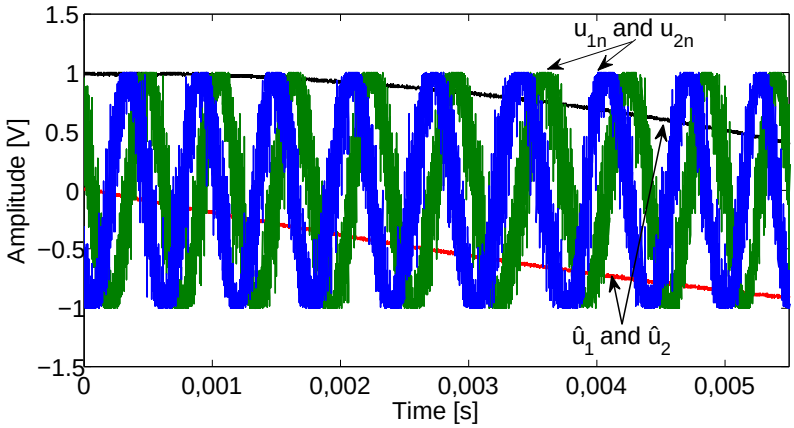

Figure 6.12: Interpolation Results for $n = 50$

Raw signals are collected using the linear encoder attached on the slider. Then, the proposed adaptive correction and look-up table based interpolation methods are used to obtain high resolution. Figure 6.11, Figure 6.12 and Figure 6.13 show the interpolation results with $n = 16$, $n = 50$ and $n = 100$, respectively. In Figure 4.6, interpolation with $n = 25$ is also given. In these figures, interpolated signals and corrected signals are shown to illustrate the performance of the presented method. In these figures, effectiveness of the correction method can be observed by looking at the signal magnitudes, phase differences and mean values of the signals. As it can be observed, both corrected signals have magnitudes of $1V$. Moreover, when one of the corrected signals is at the maximum or minimum value ($1V$ or $-1V$), the other one is at $0V$. Hence, it can be said that

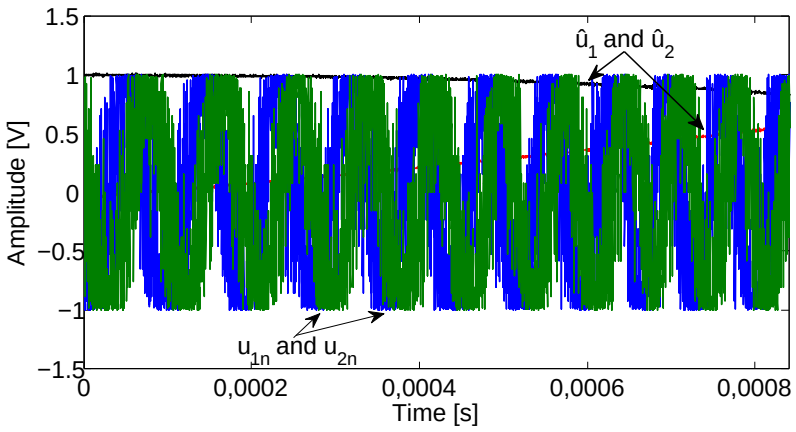

Figure 6.13: Interpolation Results for $n = 100$

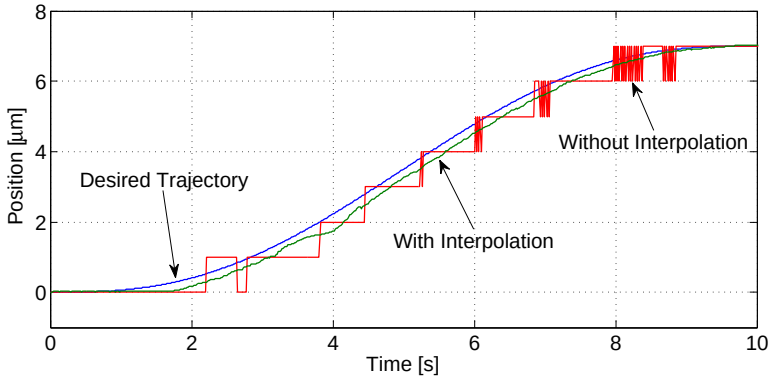

Figure 6.14: Tracking Performance of the Single Axis Slider

phase difference between the corrected signals is 90 *degrees* as desired. Similarly, performance of the interpolation can be observed from these figures by checking the signal magnitudes, phase differences and mean values of the interpolated signals. Validation tests given in Section 6.1.2 also show the effectiveness of both correction and interpolation methods presented in this thesis.

In the experiments, $N = 1000$ samples per octant is used for interpolation process. As it can be observed from the experiment results, sensitivity to noise increases with increasing interpolation number. Hence, as mentioned previously, it is very important to select a proper threshold value, ε, for binary pulse generation. With the proper selection of ε, undesired switching due to the interpolation noise can be eliminated. Therefore, resulting position value will not be

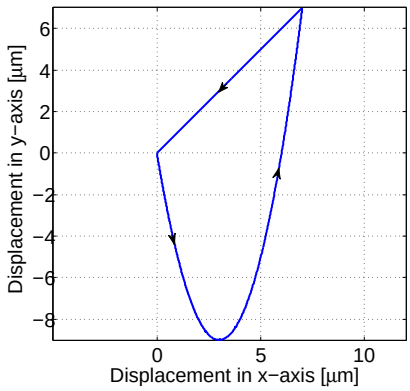

Figure 6.15: Reference Input Trajectory for Two-Axis Slider System

affected from the noise generated during the interpolation. In the experiments, this threshold value is chosen as $0.05V$. On the other hand, in order to achieve higher interpolation values (more than $n = 100$), noise in the encoder signals should be minimized by proper shielding, grounding and filtering processes.

In this section, results of the experiments on single, two and three axis slider systems are also given to illustrate the effects of encoder resolution improvement on tracking and contouring performance of the systems. Positioning performance of the single axis slider system is tested to compare the cases with and without interpolation of the encoder signals. For this purpose, same reference inputs are applied to the system. A conventional PID controller is used as a feedback controller. For the interpolation case, $n = 100$ is used so that the resolution of the measured position is $10nm$. In Figure 6.14, performance of the system for a reference input of $7\mu m$ is illustrated. In order to compare the tracking errors and obtain a smooth motion, the reference input is given as an S-curve [41]. From this figure, it is obvious that the tracking performance is increased significantly considering the focus of interest is micro/nano-meter level positioning. For no interpolation case the tracking error is $312.14nm$. On the other hand, when the encoder resolution is increased to $10nm$, the tracking error is reduced to $121.53nm$.

The encoder resolution improvement method is also successfully implemented

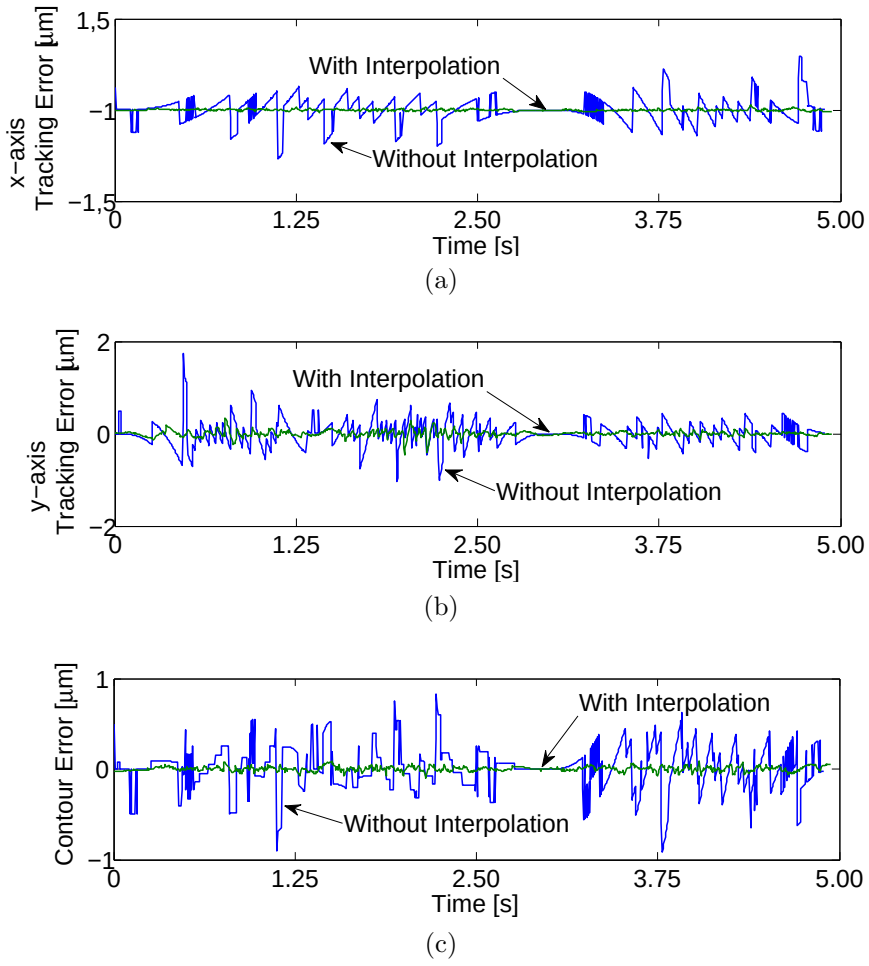

Figure 6.16: Tracking, (a) and (b), and Contouring, (c), Performance of Two-Axis Positioning System

on the two axis positioning system achieving high-tracking and contouring accuracy. For experiments conducted on two axis system, parameters in the interpolation algorithm are the same for both encoders since the adaptive feature of the correction scheme compensates the differences in the encoder signals effectively. In Figure 6.15, reference input trajectory applied to the two-axis positioning system is given. Shape of the input is designed to observe tracking and contouring performance of the system. Figure 6.16 shows the resulting tracking and contouring errors for the cases with no interpolation and interpolation with $n = 40$. Here, the contour error is defined as the distance between actual position and the nearest position on the contour. For this experiment, cross coupled control with iterative learning is implemented as controller. When there is no encoder signal interpolation, both tracking and contouring errors are at micrometer scale. However, when the encoder signal interpolation is employed, RMS of contouring error, x-axis and y-axis tracking errors are obtained as $27nm$, $21nm$ and $66nm$, respectively. Details on this study can be found in [39].

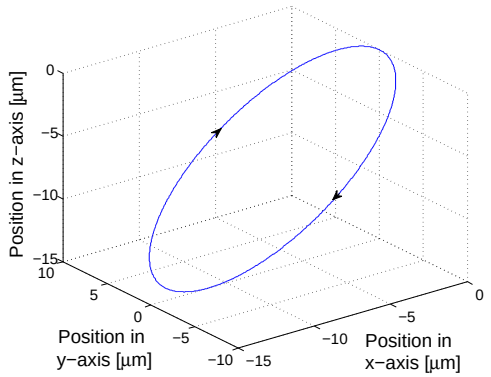

Figure 6.17: Three Dimensional Reference Input Trajectory for Three-Axis Slider System

Another experiment is conducted on three-axis positioning system to show the importance of encoder resolution improvement on tracking and contouring performance of a positioning system. Similar to the two-axis experiments, parameters in the interpolation algorithm are the same for all of three encoders. In Figure 6.17, three dimensional reference input trajectory applied to the system is given and resulting tracking and contour errors are shown in Figure 6.18 for both with and without interpolation cases. In this experiment, $n = 100$ is chosen as the

interpolation number so that the encoder resolution is $10nm$ for the interpolation case. As the controller, cross-coupled control [39] is implemented for both cases. When there is no interpolation in the encoders, tracking errors for x, y and z axis are $647.77nm$, $695.18nm$ and $1171.58nm$, respectively and the contour error is measured as $548.83nm$. However, when resolution of the encoders is increased to $10nm$, tracking errors are reduced to $82.34nm$, $95.90nm$ and $234.09nm$ for x, y and z axis. Similarly, contour error is also reduced to $83.51nm$.

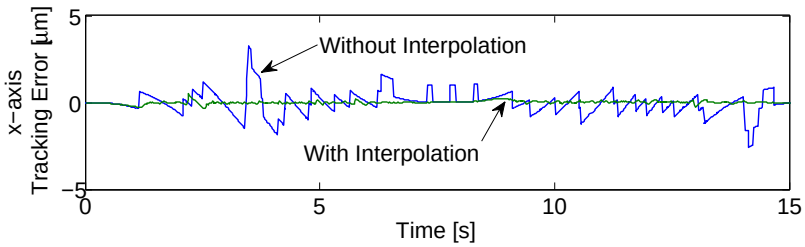

(a)

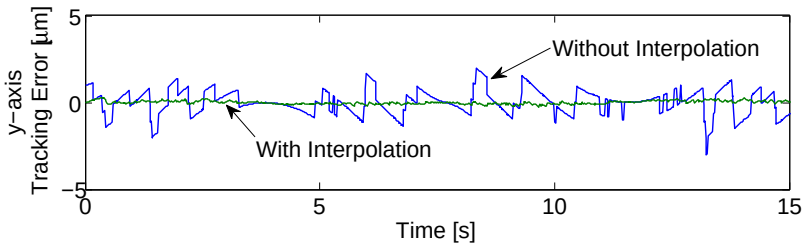

(b)

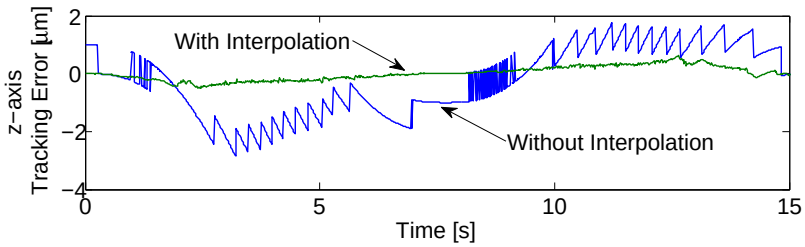

(c)

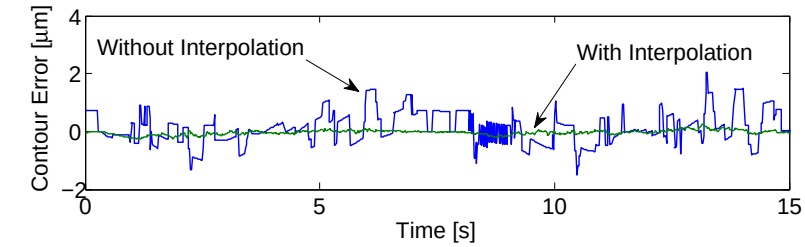

(d)

Figure 6.18: Tracking, (a), (b)and (c), and Contouring, (c), Performance of Three-Axis Positioning System

Chapter 7

Conclusion and Future Works

The goal of this work was to design a three-axis high precision positioning device that can operate in $120mm$ range for each axis. For this purpose, a modular single axis slider is designed so that three of them can be assembled to form the three-axis positioning device. Here, modularity of the single axis slider allows to be used in various configurations leading different operation spaces. In this manner, several possible configurations of single axis sliders are discussed. In the single axis slider design, permanent magnet linear motor is used as actuator and linear optical encoder is chosen as feedback sensor. Design criteria for mechanical components of the single axis slider is discussed. A counter balance system designed for the vertical arrangement of a slider in three-axis positioning system is presented.

Since the linear optical encoders have original measurement resolution of $1\mu m$, a new adaptive approach is proposed to increase the resolution. In this approach, correction of the signal errors including amplitude difference, mean offsets and quadrature phase shift errors is accomplished adaptively by using recursive least squares with exponential forgetting and resetting. Due to the adaptive characteristics of this correction method, even dynamically changing errors are effectively compensated. Then, a quick access look-up table based interpolation method is proposed for mapping of original sinusoids to high-order ones. Since the table is constructed offline, computational effort is minimal. By converting the

high-order sinusoids into binary pulses, high resolution position information is obtained. Since all of these processes are performed in software, external hardware requirements are eliminated. External validation of the method presented here is accomplished for several cases including the best resolution obtained using a differential laser vibrometer with known resolution. Limitations on the proposed method due to the practical constraints are also discussed and theoretical relations are supplied. Effectiveness of the proposed method is illustrated with the experimental results. Using the proposed encoder interpolation method, up to 100 interpolations have been accomplished successfully. As a result, $10nm$ measurement resolution is obtained with an optical encoder having $1\mu m$ original resolution. Effect of the encoder resolution improvement on positioning performance is illustrated by the experiments conducted on single, two and three-axis slider systems. Significant improvements on the tracking and contouring performance for all systems are observed. Since the encoder resolution improvement technique is adaptive, the same method is applied on different encoders on two and three axis systems without any change in the parameters.

Although nanometer level resolutions are accomplished with the presented encoder resolution improvement method, its sensitivity to noise cannot be ignored for high interpolation numbers (larger than 100). Hence, in future, sensitivity to noise can be reduced to obtain high resolution numbers by employing either a hardware or software based modification in the system. Although the presented encoder signal interpolation method is mathematically suitable for any encoders with sinusoidal outputs, it is only used for linear optical encoders so far. Hence, applicability and performance of the method can be examined on different type of sinusoidal encoders such as magnetic encoders.

In terms of the designed positioning system, only specific configurations are examined so far. Therefore, effectiveness of some other possible configurations can be tested. Moreover, three-axis positioning system presented in this thesis can be used in several applications such as micro/nano-machining in order to observe its performance under specific conditions.

Bibliography

[1] http://www.nookindustries.com/slidesystem/SlideMMSeries.cfm.

[2] http://www.physikinstrumente.com/en/products/prdetail.php?sortnr=202600.

[3] http://www.aerotech.com/product-catalog/motors/linear-motors.aspx.

[4] S. Devasia, E. E. Eleftheriou, and R. Moheimani, "A survey of control issues in nanopositioning," *IEEE Transactions on Control Systems Technology*, vol. 15, no. 15, pp. 802–823, 2007.

[5] L. Lihua, L. Yingchun, G. Yongfeng, and S. Akira, "Design and testing of a nanometer positioning system," *Journal of Dynamic Systems, Measurement, and Control*, vol. 132, no. 2, pp. 021011–6, 2010.

[6] E. Manske, T. Hausotte, R. Mastylo, T. Machleidt, K. Franke, and G. Jager, "New applications of the nanopositioning and nanomeasuring machine by using advanced tactile and non-tactile probes," *Measurement Science and Technology*, vol. 18, pp. 520–527, 2007.

[7] C. K. Pang, G. Guo, B. M. Chen, and T. H. Lee, "Self-sensing actuation for nanopositioning and active-mode damping in dual stage HDDs," *IEEE/ASME Transactions on Instrumentation and Measurement*, vol. 11, no. 3, pp. 328–338, 2006.

[8] S. O. R. Moheimani, "Invited review article: Accurate and fast nanopositioning with piezoelectric tube scanners: Emerging trends and future challenges," *Rev. Sci. Instrum.*, vol. 79, no. 7, pp. 071101–11, 2008.

[9] S. S. Aphale, S. Devasia, and S. O. R. Moheimani, "High-bandwidth control of a piezoelectric nanopositioning stage in the presence of plant uncertainties," *Nanotechnology*, vol. 19, no. 12, p. 125503, 2008.

[10] D. Y. Abramovitch, S. Hoen, and R. Workman, "Semi-automatic tuning of pid gains for atomic force microscopes," *Asian Journal of Control*, vol. 11, no. 2, pp. 188–195, 2009.

[11] N. Sclater and N. Chironis, *Mechanisms and Mechanical Devices Sourcebook*. McGraw-Hill Professional, fourth edition ed., 2006.

[12] K. K. Tan, H. Dou, Y. Chen, and T. H. Lee, "High precision linear motor control via relay-tuning and iterative learning based on zero-phase filtering," *IEEE Trans. Contr. Syst. Technol.*, vol. 9, no. 2, pp. 244–253, 2001.

[13] W. Kim and S. Verma, "Multiaxis maglev positioner with nanometer resolution over extended travel range," *ASME Journal of Dynamic Systems, Measurement, and Control*, vol. 129, pp. 777–785, Nov. 2007.

[14] http://www.physikinstrumente.com/en/products/prspecs.php?sortnr=200500.

[15] *Heidenhain - Exposed Linear Encoders*.

[16] K. K. Tan, H. X. Zhou, and T. H. Lee, "New interpolation method for quadrature encoder signals," *IEEE Transactions on Instrumentation and Measurement*, vol. 51, pp. 1073–1079, Oct 2002.

[17] K. K. Tan and K. Z. Tang, "Adaptive online correction and interpolation of quadrature encoder signals using radial basis functions," *IEEE Transactions on Control Systems Technology*, vol. 13, pp. 370–377, May 2005.

[18] D. A. Bristow and A. G. Alleyne, "A high precision motion control system with application to microscale robotic deposition," *IEEE Trans. Contr. Syst. Technol.*, vol. 16, no. 6, pp. 1008–1020, 2006.

[19] L. Xu and B. Yao, "Adaptive robust precision motion control of linear motors with negligible electrical dynamics: Theory and experiments," *IEEE/ASME Transactions on Mechatronics*, vol. 6, no. 4, pp. 444–452, 2001.

[20] B. Yao, "Adaptive robust motion control of linear motors for precision manufacturing," *Mechatronics*, vol. 12, no. 4, pp. 595–616, 2002.

[21] Y. S. Huang and C. C. Sung, "Function-based controller for linear motor control systems," *IEEE Trans. Ind. Electron.*, vol. 57, no. 3, pp. 1096–1105, 2010.

[22] P. V. D. Braembussche, J. Swevers, H. V. Brussel, and P. Vanherck, "Accurate tracking control of linear synchronous motor machine tool axes," *Mechatronics(Oxford)*, vol. 6, no. 5, pp. 507–521, 1996.

[23] D. M. Alter and C. T. Tsao, "Control of linear motors for machine tool feed drives: Design and implementation of h-optimal feedback control," *Journal of Dynamic Systems, Measurement, and Control*, vol. 118, no. ?, p. 649, 1996.

[24] D. M. Alter and C. T. Tsao, "Dynamic stiffness enhancement of direct linear motor feed drives for machining," in *Proc. IEEE American Control Conference*, 1994.

[25] J. Butterworth, L. Pao, and D. Abramovitch, "A comparison of control architectures for atomic force microscopes," *Asian Journal of Control*, vol. 11, no. 2, pp. 175–181, 2009.

[26] A. Basak, *Permanent-Magnet DC Linear Motors*. Oxford: Clarendon Press, 1996.

[27] H. Shinno, H. Yoshioka, and K. Taniguchi, "A newly developed linear motor-driven aerostatic x-y planar motion table system for nano-machining," *CIRP Annals - Manufacturing Technology*, vol. 56, no. 1, pp. 369–372, 2007.

[28] *Polytec User Manual - Vibrometer Controller for OFV-5000.*

[29] E. Ulu, N. Gecer-Ulu, and M. Cakmakci, "Adaptive correction and look-up table based interpolation of quadrature encoder signals," in *Proc. ASME Dynamic Systems and Control Conference*, (Ft. Lauderdale, FL), Oct 2012. To appear.

[30] K. P. Birch, "Optical fringe subdivision with nanometric accuracy," *Precision Engineering*, vol. 12, Oct 1990.

[31] P. L. M. Heydemann, "Determination and correction of quadrature fringe measurement errors in interferometers," *Applied Optics*, vol. 20, Oct 1981.

[32] S. Balemi, "Automatic calibration of sinusoidal encoder signals," in *Proc. 16th IFAC World Congress*, (Prague, Czech Republic), Jul 2005.

[33] H. V. Hoang and J. W. Jeon, "An efficient approach to correct the signals and generate high-resolution quadrature pulses for magnetic encoders," *IEEE Transactions on Industrial Electronics*, vol. 58, Aug 2011.

[34] N. C. Cheung, "An innovative method to increase the resolution of optical encoders in motion servo systems," in *Proc. IEEE International Conference on Power Electronics and Drive Systems*, (Hong Kong), pp. 797–900, Jul 1999.

[35] A. M. Madni, M. Jumper, and T. Malcolm, "An absolute high-performance, self-calibrating optical rotary positioning system," in *Proc. IEEE Aerospace Conference*, vol. 5, pp. 2363–2373, Mar 2001.

[36] H. T. Le, H. V. Hoang, and J. W. Jeon, "Efficient method for correction and interpolation signal of magnetic encoders," in *Proc. IEEE International Conference on Industrial Informatics*, pp. 1383–1388, Jul 2008.

[37] R. Hoseinnezhad, A. Bab-Hadiashar, and P. Harding, "Calibration of resolver sensors in electromechanical braking systems: A modified recirsive weighted least-squares approach," *IEEE Transactions on Industrial Electronics*, vol. 54, pp. 1052–1060, Apr 2007.

[38] *THK - Cross Roller Guide/Ball Guide*.

[39] N. Gecer-Ulu, E. Ulu, and M. Cakmakci, "Learning based cross-coupled control for multi-axis high precision positioning systems," in *Proc. ASME Dynamic Systems and Control Conference*, (Ft. Lauderdale, FL), Oct 2012. To appear.

[40] K. J. Astrom and B. Wittenmark, *Adaptive Control*, ch. 2, pp. 42–56. Mineola, NY: Dover Publications, 2 ed., 1995.

[41] N. Gecer-Ulu, E. Ulu, and M. Cakmakci, "Development of a moduler single-axis slider system for high precision positioning applications," in *The 15th International Conference on Machine Design and Production*, 2012.

Appendix A

Labview Implementations

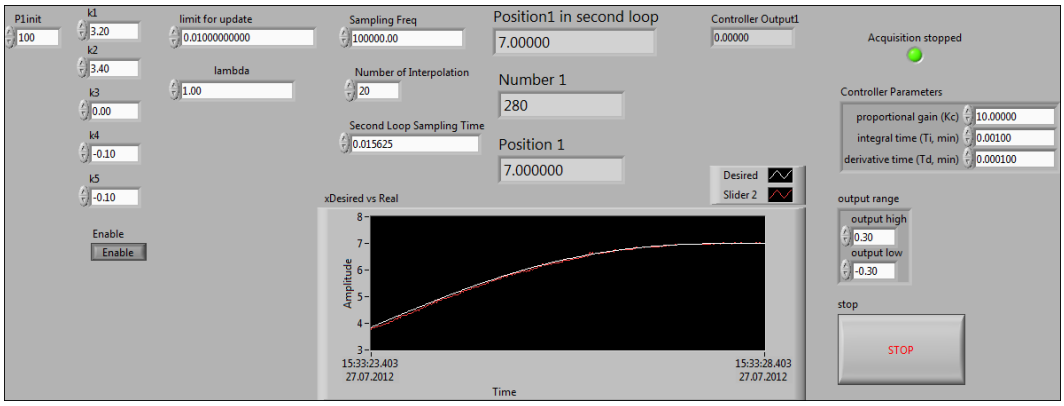

Figure A.1: Labview Front Panel for Single Axis Slider

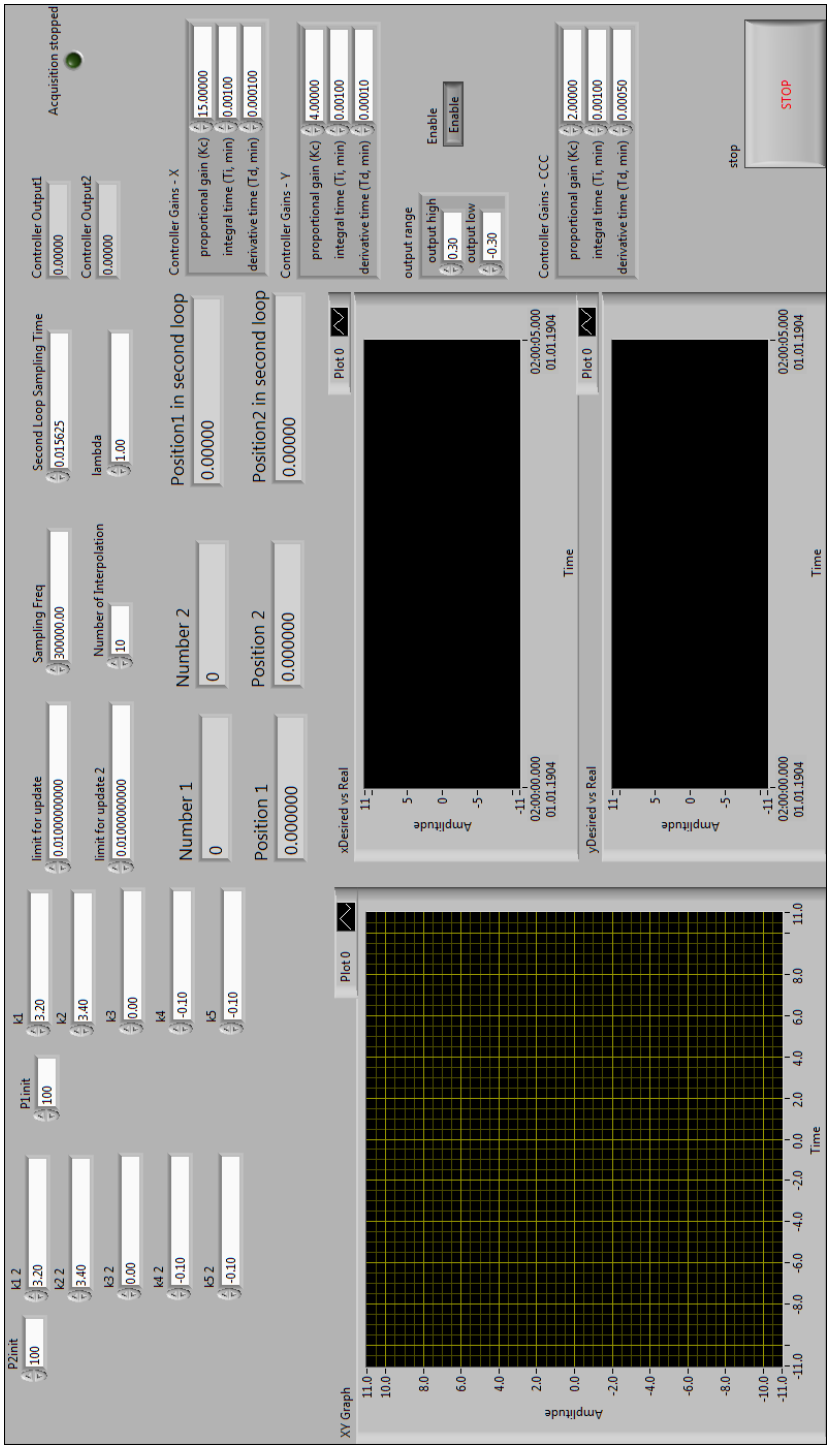

Figure A.2: Labview Front Panel for Two-Axis Slider System

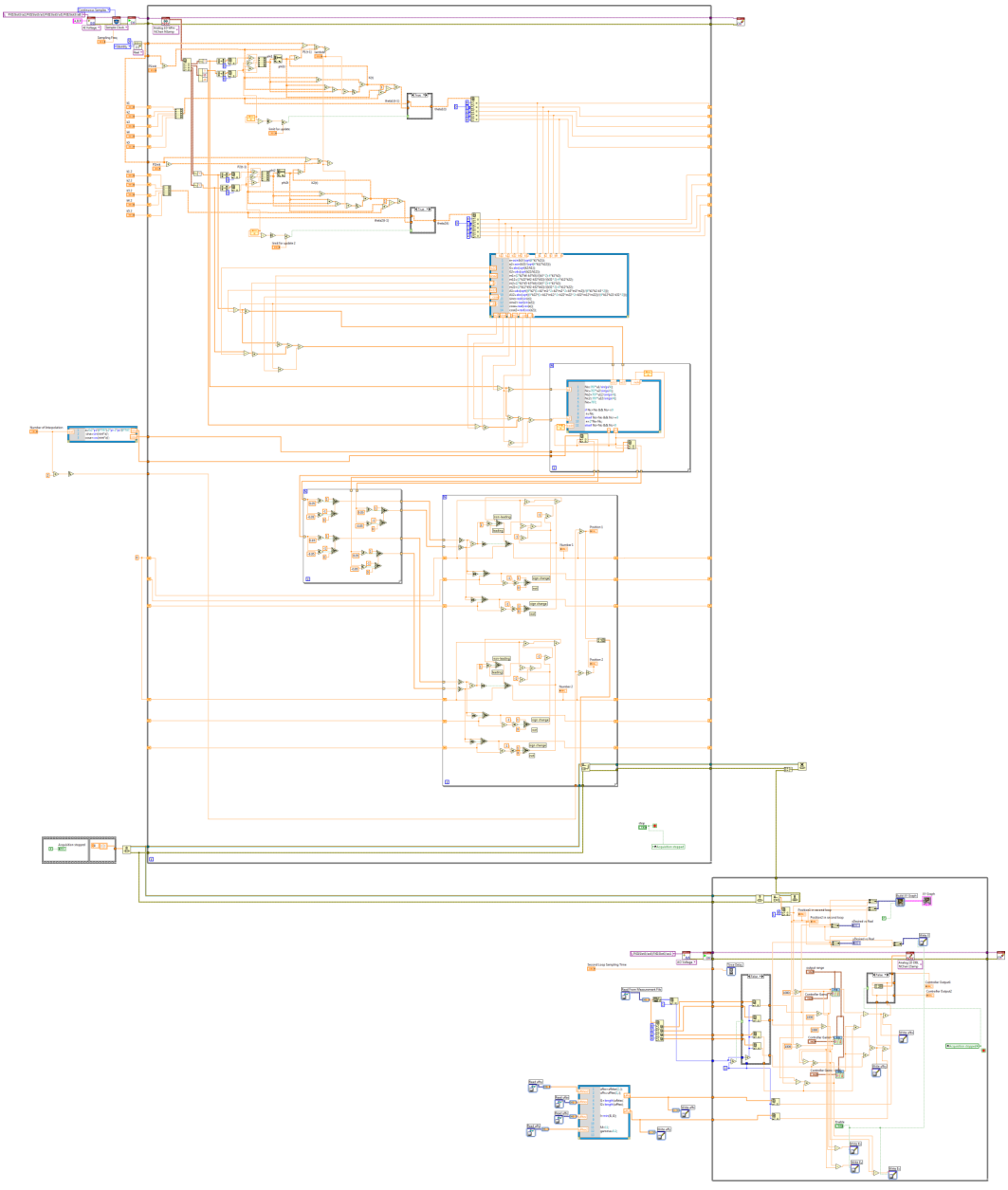

Figure A.3: Labview Implementation of Overall Control System for Two-Axis Slider System

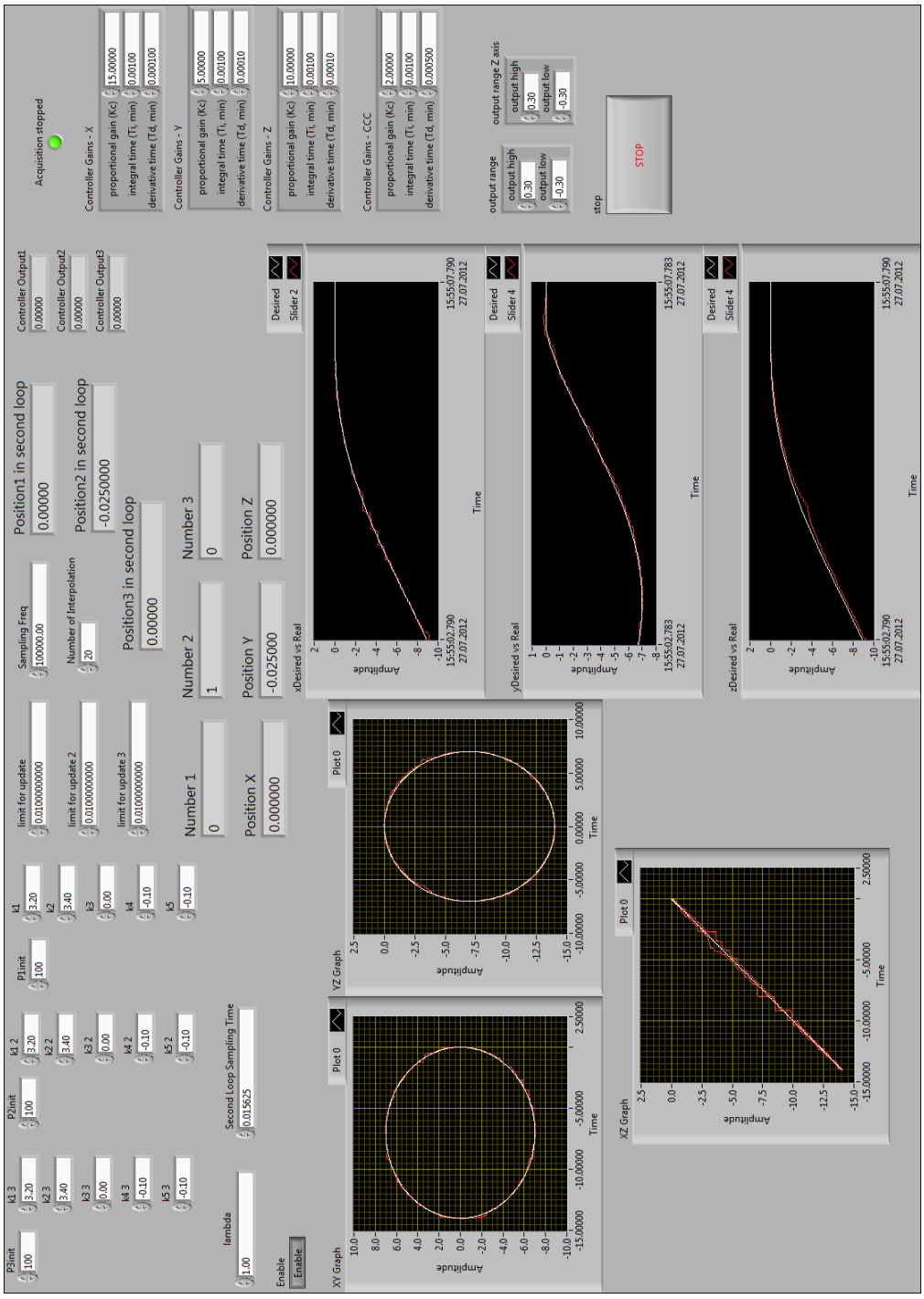

Figure A.4: Labview Front Panel for Three-Axis Slider System

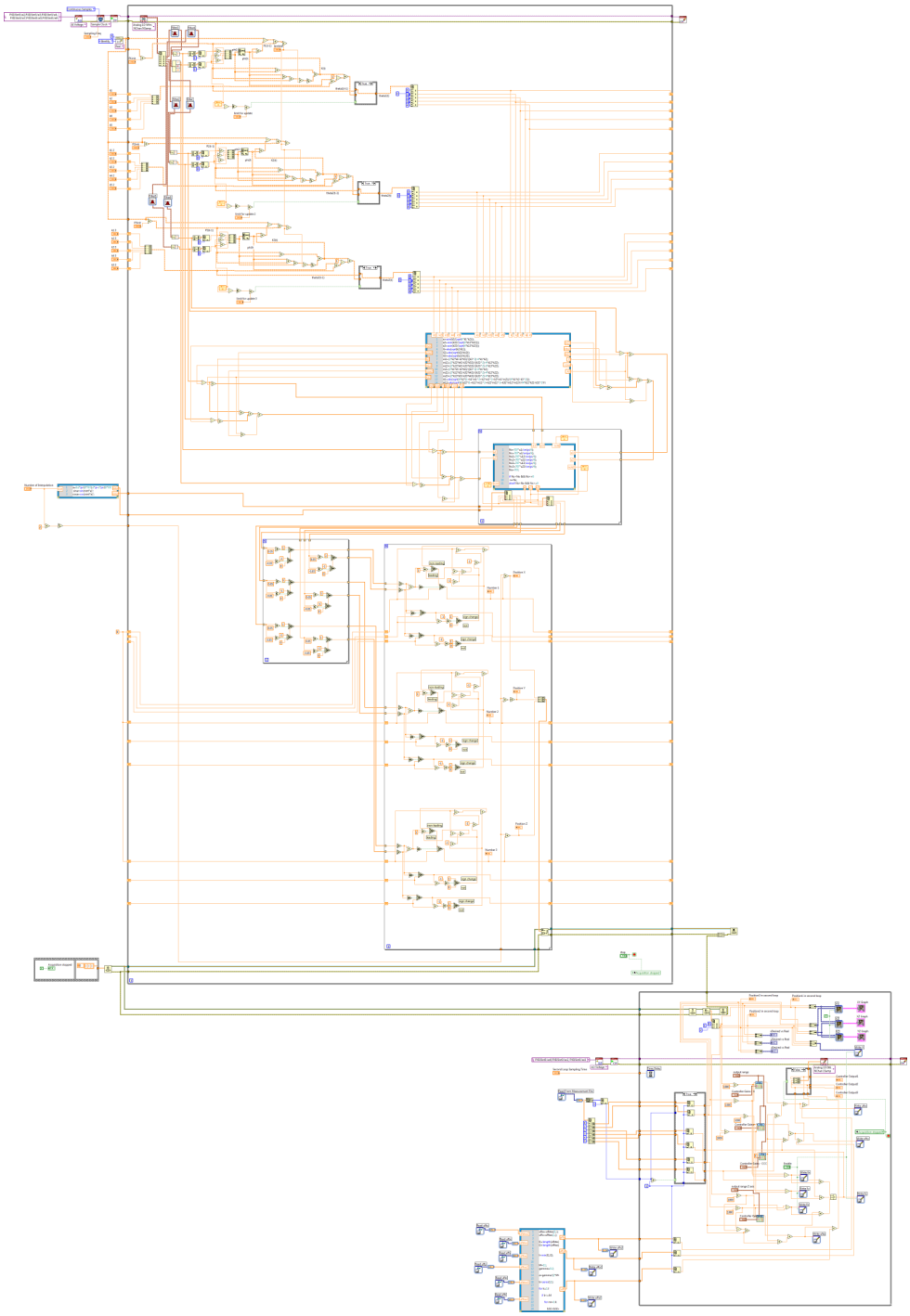

Figure A.5: Labview Implementation of Overall Control System for Three-Axis Slider System